Journal of Volcanology and Geothermal Research 286 (2014) 116–137

Contents lists available at ScienceDirect

Journal of Volcanology and Geothermal Research

journal homepage: www.elsevier.com/locate/jvolgeores

Evolution and genesis of volcanic rocks from Mutnovsky Volcano, Kamchatka

A. Simon [a,*], G.M. Yogodzinski [b], K. Robertson [c], E. Smith [c], O. Selyangin [d], A. Kiryukhin [e], S.R. Mulcahy [f], J.D. Walker [g]

[a] University of Michigan, Department of Earth and Environmental Sciences, Ann Arbor, MI 48109-1005, USA
[b] University of South Carolina, Department of Earth and Ocean Sciences, Columbia, SC 29208, USA
[c] University of Nevada Las Vegas, Department of Geoscience, Las Vegas, NV 89154, USA
[d] Research Geotechnological Center, Far Eastern Division, Russian Academy of Sciences, Petropavlovsk-Kamchatsky 683006, Russia
[e] Institute of Volcanology and Seismology, Far Eastern Division, Russian Academy of Sciences, Petropavlovsk-Kamchatsky 683006, Russia
[f] University of California Berkeley, Department of Earth and Planetary Science, Berkeley, CA 94720, USA
[g] University of Kansas, Department of Geology, Lawrence, KS 66045, USA

ARTICLE INFO

Article history:
Received 1 February 2014
Accepted 5 September 2014
Available online 19 September 2014

Keywords:
Arc volcanism
Geochemistry
Subduction
Differentiation
Fractionation
Assimilation

ABSTRACT

This study presents new geochemical data for Mutnovsky Volcano, located on the volcanic front of the southern portion of the Kamchatka arc. Field relationships show that Mutnovsky Volcano is comprised of four distinct stratocones, which have grown over that past 80 ka. The youngest center, Mutnovsky IV, has produced basalts and basaltic andesites only. The three older centers (Mutnovsky I, II, III) are dominated by basalt and basaltic andesite (60–80% by volume), but each has also produced small volumes of andesite and dacite. Across centers of all ages, Mutnovsky lavas define a tholeiitic igneous series, from 48–70% SiO_2. Basalts and basaltic andesites have relatively low K_2O and Na_2O, and high FeO* and Al_2O_3 compared to volcanic rocks throughout Kamchatka. The mafic lavas are also depleted in the light rare earth elements (REEs), with chondrite-normalized La/Sm < 1.0. Andesites have generally higher REE abundances and are more enriched in light REEs, some showing negative Eu anomalies. All samples are depleted in field strength elements (HFSEs) relative to similarly incompatible REEs (e.g., low La/Ta, Nd/Hf compared to MORB), similar to island arc volcanic rocks worldwide. Radiogenic isotope ratios (Sr, Nd, Pb, Hf) are similar for samples from all four eruptive centers, and indicate that all samples were produced by melting of a similar source mixture. No clear age-progressive changes are evident in the compositions of Mutnovsky lavas. Mass balance and assimilation-fractional crystallization (AFC) modeling of major and rare earth elements (REEs) indicate that basaltic andesites were produced by FC of plagioclase, clinopyroxene and olivine from a parental basalt, combined with assimilation of a melt composition similar to dacite lavas present at Mutnovsky. This modeling also indicates that andesites were produced by FC of plagioclase from basaltic andesite, combined with assimilation of dacite. Dacites erupted from Mutnovsky I and II have low abundances of REEs, and do not appear to be related to mafic magmas by FC or AFC processes. These dacites are modeled as the products of dehydration partial melting at mid-crustal levels of a garnet-free, amphibole-bearing basaltic rock, which itself formed in the mid-crust by emplacement of magma that originated from the same source as all Mutnovsky magmas. Lead isotope data indicate that subducted sediment is likely present in the source beneath Mutnovsky and most Kamchatka volcanoes, but uniformly radiogenic Hf and Nd in mafic samples (ε_{Nd} = 8.7–9.3, ε_{Hf} = 15.4–15.9), and significant variation in trace element ratios at nearly constant ε_{Nd} and ε_{Hf}, indicate that sediment plays a minor roll in controlling subduction trace element patterns in Mutnovsky lavas. Mafic lavas with Ba/Th > 450 require an aqueous fluid source component from subducting oceanic crust, but mixing patterns in isotope versus trace element ratio plots for Hf and the REEs (ε_{Nd} and ε_{Hf} vs. ratios with Ce, Nd and Hf) demonstrate that a source component with radiogenic Nd and Hf, and fractionated (arc-type) trace element ratios must be present in the source of Mutnovsky lavas. This source component, which is interpreted to be a partial melt of subducted basalt in the eclogite facies (eclogite melt source component), appears to be present in the source of all Kamchatka volcanoes. Cross-arc geochemical patterns at Mutnovsky and in other arc systems (Isu-Bonin, Tonga-Kermadec) suggest that the aqueous fluid component diminishes and the eclogite melt component is increased from volcanoes at the arc front compared to those in rear-arc positions.

* Corresponding author. Tel.: +1 734 647 4245; fax: +1 734 763 4690.
E-mail address: simonac@umich.edu (A. Simon).

http://dx.doi.org/10.1016/j.jvolgeores.2014.09.003
0377-0273/

1. Introduction

Volcanic rocks produced by arc volcanism provide important information about lithospheric-scale mass transfer and about the roll of subduction in the creation and recycling of continental crust (Kay, 1980; Rudnick and Fountain, 1995; Kelemen, 1995). To understand the crust–mantle system, it is important to first understand the source of arc magmas, as well as the evolutionary pathways (liquid lines of descent) that primitive arc magmas follow as they rise to the surface and are emplaced or erupted. In cases where melting of the arc crust has occurred, it is similarly important to recognize the igneous rocks that such processes create, and to document their role in shaping the geochemistry of nascent, arc-related continental crust.

The Kamchatka subduction system provides an outstanding opportunity to test ideas about the genesis and evolution of subduction-related igneous rocks (Ponomareva et al., 2007). Many Kamchatka volcanoes are highly active, and have left well preserved records of their eruptive histories (e.g., Braitseva et al., 1992; Ponomareva et al., 1998), which provide the opportunity to study magmatic evolution on a variety of time scales (e.g., Turner et al., 1998, 2007; Dosseto et al., 2003). Kamchatka volcanic rocks are dominantly mafic (Ponomareva et al., 2007) including many with primitive, high-Mg-number compositions (molar Mg/Mg + Fe, or Mg# > 0.60) that have been largely unaffected by crust-level processes (Kersting and Arculus, 1995; Hochstaedter et al., 1996; Volynets et al., 1997; Portnyagin et al., 2007a, 2007b; Bryant et al., 2011; Gorbach and Portnyagin, 2011a, 2011b). Xenoliths from several locations also provide constraints on the composition of the mantle lithosphere that forms the foundation of the Kamchatka arc (Widom et al., 2003; Bryant et al., 2007; Saha et al., 2005; Ishimaru et al., 2007). Finally, along-strike changes in tectonic conditions and related spatial–geochemical patterns provide clear constraints on the source of Kamchatka magmas, and processes occurring at depth within the subduction zone (Yogodzinski et al., 2001; Portnyagin et al., 2005).

In this paper we present the results of a geochemical study of volcanic rocks from Mutnovsky Volcano, which is located on the eastern volcanic front in southern Kamchatka. A unique feature of Mutnovsky is that it has produced mostly low K, basaltic lavas that have depleted rare earth element patterns, similar to the classic island arc tholeiites of Jakes and Gill (1970). Basalts of this type are common in the western Pacific island arcs, but it is unusual to find such compositions in a transitional subduction system such as Kamchatka, which is formed on the margin of a continent. This is the first geochemical investigation to characterize the nature and evolution of all four eruptive centers at Mutnovsky. Data presented in this paper expand upon and complement the comparisons of Mutnovsky and nearby Gorely Volcano which lies just 15 km to the west of Mutnovsky, a short distance to the rear arc (Selyangin, 1993; Duggen et al., 2007).

2. Regional geology & history of Mutnovsky

Mutnovsky Volcano is located 70 km southwest of Petropavlovsk-Kamchatsky on the Kamchatka Peninsula in eastern Russia (Fig. 1). Mutnovsky is part of the Eastern Volcanic Front, which is the easternmost of the three major volcanic chains in Kamchatka, which are produced by northwest-directed subduction of the Pacific Plate at a rate of ~8 cm/yr beneath the Okhotsk microplate (Moore et al., 1992; Gorbatov, 1997; Gorbatov et al., 1999; Lees et al., 2007). The other volcanic chains, from west to east, are the Sredinny Range and the Central Kamchatka Depression (Fig. 1). These belts, from west to east, represent the evolution of the volcanic arc over approximately the past 30 Ma (Avdeiko et al., 2007). Tomographic images of the P-wave velocity structure of the mantle wedge indicate that volcanoes along the eastern margin of the volcanic front of southern Kamchatka, including Mutnovsky, are located ~90–100 km above the top of the subducting slab, whereas the neighboring, active, rear-arc Gorely volcano, located ~15 km west of Mutnovsky, is located ~120 km above the subducting slab (Gorbatov et al., 1999). Cross-arc changes in abundances and ratios among incompatible elements from Mutnovsky to Gorely, and the positions of these volcanoes, relative to the surface of the subducting plate at depth were interpreted by Duggen et al. (2007) to play a major role in controlling the geochemistry of erupted magmas.

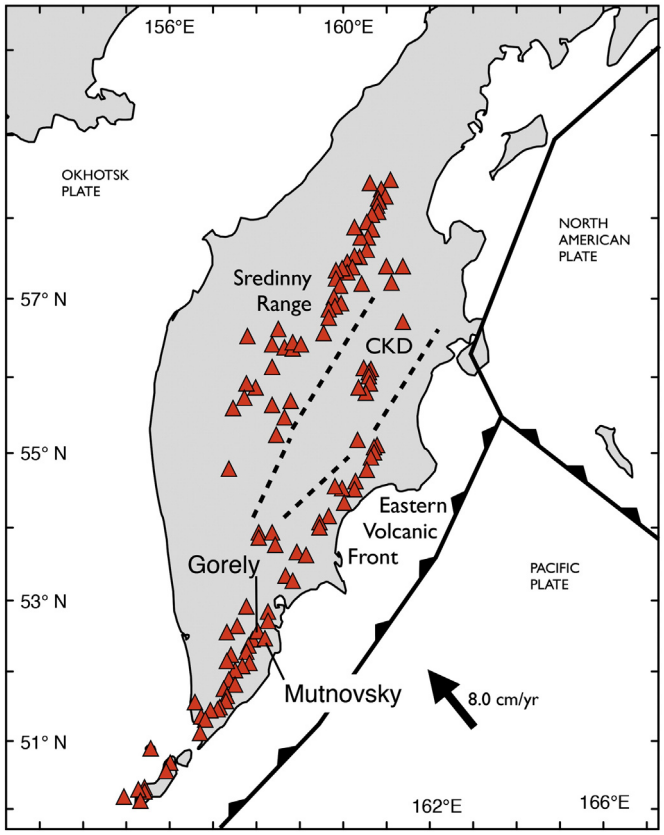

Fig. 1. Map of the Kamchatka area, showing the locations of major features mentioned in the text. The red triangles mark the locations of Holocene volcanoes from the Smithsonian Global Volcanism database. Volcanic belts of Kamchatka are also shown — the Sredinny Range, the Central Kamchatka Depression (CKD) and the Eastern Volcanic Front. The dashed lines mark the approximate boundaries of the Central Kamchatka Depression. The bold arrow shows the Pacific–North America plate convergence direction and rate (308° and 8.1 cm/yr) based on the NUVEL-1 model and determined using the online Unavco Plate Motion Calculator. (For interpretation of the references to color in this figure legend, the reader is referred to the web version of this article.)

Mutnovsky is a complex of 4 composite volcanic cones, referred to as Mutnovsky I–IV, which have been active since the late Pleistocene (Fig. 2; Selyangin, 1993, 2009). There are no radiometric ages for Mutnovsky rocks, but the ages of the Mutnovsky eruptive centers and their deposits have been located in regional and local stratigraphic frameworks of glacial deposits and tephra that is well constrained by ^{14}C dating (Ponomareva et al., 2007). The following field and geologic descriptions are summarized from Selyangin (1993, 2009).

Activity at Mutnovsky I, the oldest of the four Mutnovsky centers, commenced 60–80 ka ago. Mutnovsky I produced basalt, basaltic andesite, andesite and dacite lavas and pyroclastic rocks with a total volume of approximately 58 km^3. Existing data, including new data presented in this paper, indicate there is no systematic change in volcanic rock composition with stratigraphic position for lavas and pyroclastic materials produced by Mutnovsky I volcanism (Selyangin, 1993). A well-exposed swarm of north–south striking, and steeply dipping basalt dikes in the wall of Kleshnya ridge in the NE sector of the cone, is interpreted to represent part of the Mutnovsky I magma feeder system that has been uplifted and exposed by erosion. Mutnovsky II, which formed between approximately 30 and 40 ka, is located 3 km southeast of the Mutnovsky I center. Mutnovsky II produced approximately 24 km^3 of lava and pyroclastic material. Compositions of Mutnovsky II

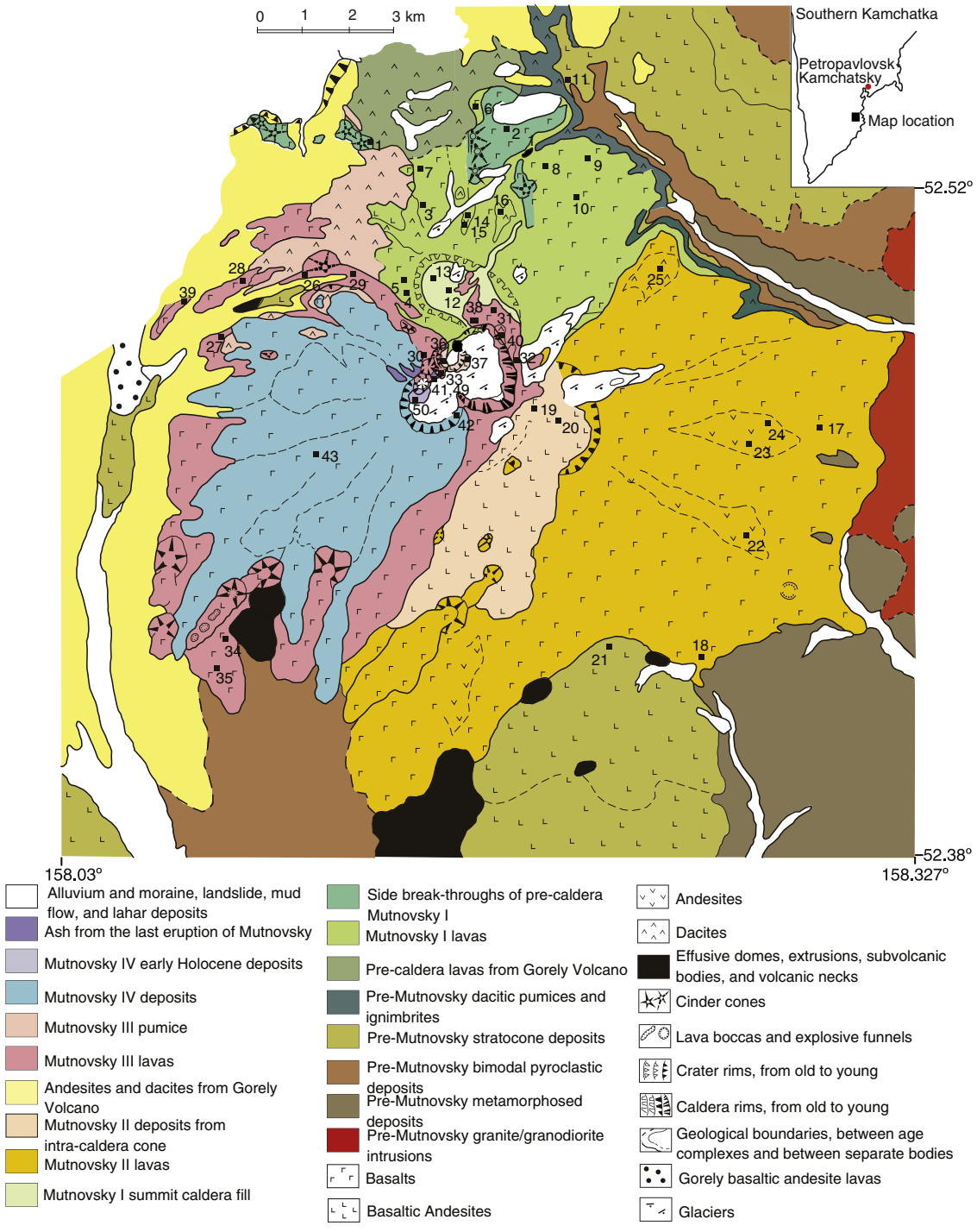

Fig. 2. Geological map of Mutnovsky volcano, modified from Selyangin (2009) with original computer graphics by E.M. Gazzaeva. Inset shows location of map in Kamchatka. Squares with numbers correspond to sample locations, as numbered in Table 1. Numbers on map indicate location of samples in Table 1.

volcanic rocks are variable from basalt to dacite and are broadly similar to those produced by Mutnovsky I. Activity at Mutnovsky II also produced parasitic cones on its flanks similar in composition to those at Mutnovsky I.

Mutnovsky III, which is located between I and II (Fig. 2) erupted a relatively small volume of volcanic rock (~5 km^3) compared to the older centers. The Mutnovsky III center is composed of alternating flows and tephra with parasitic cones on its flanks, similar to Mutnovsky I and II. Mutnovsky III is also locally cut by mafic dikes, and a portions of the center is hydrothermally altered. Volcanic rock compositions at Mutnovsky III, are variable from basalt to rhyodacite. The 1.5 by 2.0-km diameter summit caldera at Mutnovsky III (Fig. 2), which was produced by an eruption of 2.0–2.5 km^3 of pumice, is now partially filled with lava flows from Mutnovsky IV. Mutnovsky III also contains an intra-caldera basaltic-andesite cone and a rhyodacite extrusion. The end of Mutnovsky III activity in the caldera was marked by the eruption of a dacite dome that was dated using the local tephra stratigraphy, and constrained by ^{14}C dating, to have occurred approximately 4000 years ago (Selyangin, 1993).

Mutnovsky IV is the youngest of the Mutnovsky composite cones, and has been active for about 11 ka (Selyangin, 1993). Mutnovsky IV, which is located 1 km south–southwest of the younger Mutnovsky

centers (Fig. 2), has erupted a total volume of 3.8 km^3. Mutnovsky IV has produced lavas and pyroclastic material of basalt and basaltic andesite only. Intermediate-composition and higher silica deposits are not present at Mutnovsky IV. There is a 1.3 km-diameter crater at the summit of the cone, which is either a caldera or a small collapse feature. This crater is mostly filled with glacial deposits. The youngest volcanic deposits in the crater are from a historic eruption (2000 AD) of basaltic andesite scoria and pyroclastic material.

3. Analytical methods

Whole-rock samples were collected from lava flows and pyroclastic deposits from all four of the Mutnovsky eruptive centers. Available sample locations are listed in Table 1. Petrographic descriptions are provided in Electronic Appendix **A**. All images in the appendix were acquired under cross-polarized light. A representative piece of each sample was reduced in a jaw-crusher to pieces less than 5 mm in long dimension. These were washed in purified water, dried, and powdered in an alumina-ceramic grinding container using a Spex shatterbox. Major element analyses of rock powders were performed at Activation Laboratories in Ontario, Canada on a Varian Vista 735 ICPOES, using a lithium-borate fusion/dissolution method. Results of major element analyses are reported in Table 1, and QA/QC data are reported in Electronic Appendix B.

Approximately 40 mg of sample powder was digested for whole-rock trace element analysis by ICPMS at the University of South Carolina. The samples were digested in screw-capped Teflon capsules placed on a hotplate overnight at ~90 °C. Acids used in the digestion step, which were purified in-house by sub-boiling distillation, were a 3:1 mixture of HF:HNO_3. Digested samples were dried gently and then re-dissolved in concentrated HNO_3 twice. These steps were generally sufficient to remove fluoride precipitates from most samples. An additional dissolution and dry-down cycle in concentrated HNO_3 was needed for a few samples. The USGS standard reference materials AGV-1 and BCR-2 were prepared using the same steps. The dissolved samples (clear of visible precipitates or other solids) were diluted 3000 times the initial powder weight with de-ionized water containing 25 ppb of In, which was used as an internal drift monitor. Abundances of 26 trace elements were measured at the University of South Carolina on a Varian 820-MS quadrupole ICPMS. The instrument was run in peak-hopping mode with a dwell time of 50,000 μs. Blank solutions were measured in each analytical run. Unknown solutions were bracketed by AGV-1, which was analyzed after every five unknown solutions throughout each run. Blank-corrected and indium-normalized count rates for unknowns were drift corrected based on a linear interpolation of count rates between bracketing AGV-1 solutions (Cheatham et al., 1993; Kelley et al., 2003). Count rates for unknowns were quantified against the AGV-1 standard, using reference values from Kelley et al. (2003) and from the GeoRem database (Yogodzinski et al., in press). Small corrections (usually <2%) were applied to adjust for differences in rock powder and solution weights. Trace element concentrations in unknown solutions were corrected against results for BCR-2, which was included as an unknown in each analytical run. Repeat analyses of USGS reference standards DNC-1, W-2 and BHVO-1 indicate that analytical precision and accuracy for the method are less than 3% RSD for most elements. Additional instrument settings, standard values and results are provided in Yogodzinski et al. (in press). Results of ICPMS trace element analyses are reported here in Table 1.

Whole-rock Sr, Nd, Pb and Hf isotope analyses were performed on the most and least evolved samples, based on highest and lowest Mg# (mol [Mg/(Mg + Fe)]) and SiO_2 concentrations of samples from each eruptive center. Strontium and Nd isotopes were analyzed at the University of Kansas (KU) by using thermal ionization mass spectrometry (TIMS). Analyses for Sr and Nd (both run as metal) were performed by using a VG Sector 54, with typical internal and external precisions of ±20 ppm (2σ). Samples were prepared for analysis by standard HF–HNO_3 and HCl dissolution techniques. Elemental separation was done by using ion exchange columns. Strontium was isolated and rare earth elements collected by using cation exchange columns with Biorad resin. Neodymium and Sm were purified in Eichrome LN spec resin columns. Strontium ratios are referenced to a value of 0.710250 for the $^{87}Sr/^{86}Sr$ ratio of NBS987 after correcting for fractionation using $^{86}Sr/^{88}Sr = 0.1194$. The measured laboratory value was 0.710245 ± −0.0007 to 0.0009% (SDOM) for NBS987 over the period of analysis (23 standard runs). Neodymium ratios were corrected with a KU internal standard (using a value of 0.511905) that is tied to LaJolla Nd by using a value of 0.511860 for the $^{143}Nd/^{144}Nd$ of LaJolla. Fractionation-correction was performed by using $^{146}Nd/^{144}Nd = 0.7219$. Measured laboratory value was 0.511906 ± −0.0007 to 0.0009% (SDOM) for the KU $^{143}Nd/^{144}Nd$ standard, based on 20 standard runs.

The Pb and Hf isotope data were generated by using a Thermo Scientific NEPTUNE Plus multi-collector-ICP-MS in the Center for Elemental Mass Spectrometry at the University of South Carolina. Hand-picked rock chips were rinsed in de-ionized water, sonicated and dried. The cleaned chips were then leached with 6 N HCl in sealed, teflon capsules at ~120 °C for one hour. The resulting leachate was decanted and the samples were rinsed three times with 18 MΩ H_2O. The leached rock chips were then digested in ~6 mL of a 3:1 mixture of HF:HNO_3 on a hotplate at ~90 °C for 24 h. The digested samples were dissolved in ~1 mL of 2 N HBr and evaporated to dryness at ~90 °C on a hotplate. This step was repeated twice more. The samples were then placed on BioRad AG-1 X8 anion-exchange resin in teflon micro-columns. The Pb fraction was removed from the rock matrix by the addition of two separate mixtures of 2.5 N HNO_3 and 2 N HBr to the column (2:1 and 2:0.15). The eluted Pb fractions were passed through the columns a second time using the same steps for additional cleaning. Isotope ratios were measured on the Thermo Fisher Neptune in the Center for Elemental Mass Spectrometry at the University of South Carolina. Lead isotope samples were spiked with thallium to monitor in-run mass fractionation of Pb isotopes (White et al., 2000). Seventeen analyses of the NBS981 standard measured by this method produced values of $^{206}Pb/^{204}Pb = 16.9390 \pm 0.0037$, $^{207}Pb/^{204}Pb = 15.4924 \pm 0.0046$, and $^{208}Pb/^{204}Pb = 36.7037 \pm 0.0153$ (2 std. dev.). Results for Pb isotopes were corrected against accepted values for BCR-2 as reported in Weis et al. (2006). Hafnium isotopes samples were prepared from rock powders used for ICPMS trace elements. Initial sample digestion followed the procedure previously described for Pb. Separation of Hf was done by ion chromatography following the method of Münker et al. (2001). Instrumental mass fractionation was corrected based on a $^{179}Hf/^{177}Hf$ value of 0.7325. Isotopes ^{172}Yb and ^{175}Lu were monitored and corrections were made using the instrument software. Measurements of the JMC-475 Hf standard, which were made in the same run as the samples reported here, produced an average $^{176}Hf/^{177}Hf$ value of 0.282134 ± 0.000003 (2 standard deviations, n = 9). The $^{176}Hf/^{177}Hf$ values of samples reported in Table 2 are corrected against a reference value of 0.282160 for the JMC-475 standard (Chauvel & Blichert-Toft, 2001).

Oxygen isotope analyses were performed on olivine phenocrysts, which were separated by handpicking while under observation on a binocular microscope, by using CO_2-laser fluorination on a Finnigan MAT 253 mass spectrometer, as described in Bindeman (2008), at the University of Oregon stable isotope lab.

4. Results

4.1. Major and trace elements

Mutnovsky lavas span the compositional range from basalt to dacite, from 48.7 to 69.4% SiO_2 (Fig. 3; Table 1). Based on the criteria of Miyashiro (1974), Mutnovsky samples of all ages and from all centers define a tholeiitic igneous series with FeO*/MgO generally increasing with increasing SiO_2 (Fig. 3). By volume, Mutnovsky lavas are

Table 1
Whole-rock major and trace element results for Mutnovsky lavas.[a]

Sample	M1-04-08	M1-05-08	CM-19	CM-33	CM-105	M1-09-08	CM-48	CM-92a	CM-97a	CM-33a	M1-06-08	CM-4a	CM-5
Center	Mutn. I	Mutn. I	Mutn. I	Mutn. I	Mutn. I	Mutn. I	Mutn. I	Mutn. I	Mutn. I	Mutn. I	Mutn. I	Mutn. I	Mutn. I
Map #	1	2	3	4	5	6	7	8	9	10	11	12	13
Location	52.4919	52.4918				52.5002					52.4985		
	158.1479	158.1479				158.1558					158.1624		
SiO_2	53.14	51.67	52.42	52.59	51.06	51.23	50.92	50.94	51.44	58.08	54.08	55.13	53.95
TiO_2	1.34	1.22	1.42	1.06	1.42	1.33	1.31	1.13	1.11	1.16	1.34	0.91	1.22
Al_2O_3	18.65	19.81	19.53	23.00	17.73	17.54	17.46	20.98	18.07	18.90	17.61	18.45	18.72
FeO[a]	10.81	9.89	9.93	7.54	10.42	11.83	11.96	9.15	10.01	8.20	10.80	7.62	9.18
MnO	0.20	0.19	0.18	0.21	0.21	0.24	0.23	0.21	0.16	0.19	0.23	0.16	0.16
MgO	3.43	3.18	3.46	3.24	5.71	4.76	4.89	3.73	7.29	2.39	3.50	4.76	4.00
CaO	8.37	10.03	8.91	8.73	9.80	9.22	9.54	10.24	8.78	6.03	8.22	8.37	8.61
Na_2O	3.29	3.42	3.35	2.88	2.92	3.21	3.12	2.76	2.45	3.70	3.50	3.61	3.17
K_2O	0.55	0.41	0.55	0.60	0.52	0.42	0.36	0.74	0.55	1.12	0.45	0.78	0.74
P_2O_5	0.22	0.18	0.24	0.15	0.21	0.22	0.21	0.12	0.13	0.22	0.27	0.20	0.25
Mg#	0.36	0.36	0.38	0.43	0.49	0.42	0.42	0.42	0.56	0.34	0.37	0.53	0.44
Rb	7.06	4.95	5.35	6.86	2.79	5.66	5.26	5.83	8.09	13.2	3.34	7.35	10.1
Sr	386	399	423	420	511	413	404	412	477	402	451	410	462
Y	27.8	31.9	32.8	27.2	29.1	29.2	28.1	27.5	25.4	35.4	46.1	34.8	38.9
Zr	67.2	63.0	62.2	52.1	57.0	60.3	57.0	49.6	63.8	74.4	84.4	81.7	70.3
Nb	1.33	1.07	1.05	1.20	1.11	1.20	1.13	0.85	1.36	1.70	1.95	1.62	1.47
Cs	0.492	0.409	0.228	0.339	0.257	0.442	0.409	0.350	0.495	0.678	0.233	0.375	0.778
Ba	179	154	164	164	174	164	149	151	229	274	282	277	242
La	4.44	4.30	4.42	5.39	4.63	4.77	4.38	4.01	5.63	7.36	6.46	6.89	6.55
Ce	12.3	12.8	13.1	13.4	13.9	13.2	12.5	11.4	15.1	18.8	17.8	19.4	18.7
Pr	2.17	2.33	2.39	2.43	2.51	2.34	2.23	2.07	2.47	3.12	3.05	3.34	3.24
Nd	11.8	13.1	13.5	12.7	13.6	12.6	12.2	11.4	12.5	16.1	16.4	17.1	17.0
Sm	3.67	4.12	4.27	3.70	4.13	3.85	3.76	3.56	3.55	4.71	5.12	4.95	5.07
Eu	1.20	1.35	1.44	1.21	1.36	1.25	1.22	1.18	1.20	1.52	1.89	1.53	1.65
Gd	4.38	5.05	5.01	4.22	4.95	4.67	4.40	4.24	4.19	5.41	6.72	5.73	6.24
Tb	0.717	0.827	0.850	0.704	0.818	0.749	0.732	0.704	0.707	0.901	1.20	0.983	1.05
Dy	4.65	5.25	5.44	4.46	5.22	4.74	4.67	4.52	4.51	5.78	7.86	6.32	6.75
Ho	0.962	1.09	1.13	0.923	1.07	0.985	0.969	0.944	0.930	1.20	1.66	1.30	1.41
Er	2.70	3.04	3.18	2.59	3.01	2.73	2.71	2.63	2.64	3.40	4.80	3.70	3.96
Tm	0.412	0.462	0.484	0.396	0.449	0.412	0.405	0.396	0.396	0.524	0.725	0.567	0.601
Yb	2.78	3.10	3.25	2.64	2.88	2.74	2.75	2.68	2.61	3.52	4.71	3.75	3.89
Lu	0.422	0.464	0.497	0.400	0.455	0.415	0.416	0.401	0.413	0.540	0.726	0.587	0.617
Hf	2.19	2.12	2.11	1.72	1.87	1.95	1.90	1.70	1.96	2.45	2.56	2.58	2.28
Ta	0.076	0.061	0.060	0.073	0.063	0.065	0.063	0.046	0.086	0.106	0.111	0.097	0.085
Pb	4.09	3.05	3.87	3.66	3.55	3.78	3.51	3.43	4.82	6.27	5.98	5.92	5.50
Th	0.416	0.276	0.283	0.432	0.278	0.304	0.295	0.319	0.518	0.737	0.470	0.643	0.534
U	0.179	0.138	0.150	0.183	0.124	0.145	0.145	0.170	0.239	0.326	0.235	0.269	0.247

Sample	CM-24	M1-02-08	CM-47	CM-156	CM-169a	CM-187	CM-186	CM-142	CM-147	CM-154	CM-155	CM-113	M3-03-08
Center	Mutn. I	Mutn. I	Mutn. I	Mutn. II	Mutn. II	Mutn. II	Mutn. II	Mutn. II	Mutn. II	Mutn. II	Mutn. II	Mutn. II	Mutn. III
Map #	14	15	16	17	18	19	20	21	22	23	24	25	26
Location		52.4691											52.4788
		158.1624											158.1192
SiO_2	60.73	61.04	65.52	49.55	52.52	52.29	54.58	54.51	60.98	63.90	58.37	68.51	51.66
TiO_2	1.03	0.95	0.92	1.19	1.40	1.23	1.38	1.34	1.28	1.02	1.48	0.48	1.16
Al_2O_3	18.28	17.13	16.25	18.98	18.16	19.03	17.44	17.68	16.63	16.28	16.03	14.84	18.22
FeO[a]	6.20	7.14	5.41	9.68	10.29	9.45	9.94	9.48	7.40	5.89	9.53	4.79	11.34
MnO	0.16	0.16	0.15	0.31	0.26	0.15	0.18	0.23	0.16	0.21	0.21	0.11	0.21
MgO	2.23	2.30	1.64	6.51	4.66	4.60	4.01	3.88	2.00	1.41	2.70	1.07	4.68
CaO	5.59	5.78	4.07	11.01	8.97	9.50	8.04	8.30	4.83	4.34	6.05	3.36	9.06
Na_2O	4.42	3.94	3.81	2.13	3.02	2.87	3.39	3.56	4.72	5.13	3.95	4.62	3.02
K_2O	1.04	1.29	2.01	0.49	0.55	0.68	0.80	0.73	1.54	1.50	1.32	2.13	0.45
P_2O_5	0.32	0.27	0.22	0.15	0.17	0.19	0.24	0.29	0.46	0.32	0.35	0.10	0.21
Mg#	0.39	0.36	0.35	0.55	0.45	0.46	0.42	0.42	0.32	0.30	0.34	0.28	0.42
Rb	14.6	40.4	37.8	4.29	5.93	6.05	9.04	8.30	18.1	21.4	15.1	21.1	4.36
Sr	374	392	317	476	456	500	478	474	407	350	411	200	477
Y	42.1	43.2	40.4	26.4	29.2	31.2	40.8	38.1	57.3	56.6	52.4	20.3	23.3
Zr	122	132	192	53.7	61.5	71.5	94.9	94.2	160	193	153	122	50.2
Nb	2.46	2.76	3.59	1.07	1.18	1.48	1.95	1.94	3.56	3.95	3.16	2.75	1.14
Cs	0.269	1.58	2.51	0.415	0.520	0.246	0.474	0.607	1.22	1.46	0.737	2.38	0.363
Ba	415	390	652	166	200	196	253	250	502	591	451	696	168
La	8.21	9.75	13.2	4.23	4.99	5.59	7.52	7.12	14.0	14.0	11.0	8.51	4.30
Ce	23.9	26.1	33.8	12.4	14.4	16.5	22.0	21.2	37.7	38.3	32.0	20.9	12.0
Pr	3.82	4.27	4.99	2.21	2.51	2.85	3.79	3.60	6.23	6.06	5.29	2.69	2.02
Nd	19.3	21.8	23.1	11.9	13.4	15.0	19.8	18.9	31.2	29.8	27.0	11.7	10.8
Sm	5.62	6.16	5.97	3.65	4.02	4.41	5.75	5.48	8.44	8.09	7.68	2.86	3.24
Eu	1.83	1.99	1.54	1.21	1.34	1.40	1.72	1.64	2.24	2.14	2.15	0.900	1.18

Table 1 (*continued*)

Sample	CM-24	M1-02-08	CM-47	CM-156	CM-169a	CM-187	CM-186	CM-142	CM-147	CM-154	CM-155	CM-113	M3-03-08
Center	Mutn. I	Mutn. I	Mutn. I	Mutn. II	Mutn. II	Mutn. II	Mutn. II	Mutn. II	Mutn. II	Mutn. II	Mutn. II	Mutn. II	Mutn. III
Map #	14	15	16	17	18	19	20	21	22	23	24	25	26
Location		52.4691											52.4788
		158.1624											158.1192
Gd	6.59	7.03	6.66	4.38	4.81	5.20	6.77	6.47	9.71	9.25	8.84	3.14	3.85
Tb	1.13	1.21	1.11	0.735	0.813	0.879	1.14	1.08	1.60	1.53	1.46	0.539	0.671
Dy	7.36	7.68	7.00	4.74	5.23	5.61	7.22	6.91	10.0	9.73	9.26	3.48	4.32
Ho	1.53	1.58	1.44	0.984	1.09	1.16	1.50	1.43	2.08	2.02	1.92	0.737	0.888
Er	4.42	4.63	4.12	2.79	3.08	3.29	4.25	4.05	5.89	5.81	5.45	2.19	2.52
Tm	0.686	0.690	0.635	0.419	0.464	0.493	0.642	0.611	0.891	0.892	0.824	0.351	0.376
Yb	4.59	4.61	4.18	2.70	3.02	3.22	4.17	3.99	5.76	5.84	5.41	2.46	2.46
Lu	0.732	0.705	0.671	0.430	0.480	0.513	0.668	0.635	0.928	0.943	0.860	0.416	0.374
Hf	3.77	3.94	5.32	1.76	2.04	2.30	3.01	3.00	4.82	5.46	4.56	3.69	1.59
Ta	0.145	0.169	0.261	0.060	0.069	0.082	0.107	0.106	0.200	0.219	0.172	0.272	0.063
Pb	7.47	8.85	12.8	3.76	4.83	4.63	5.28	5.88	11.1	12.2	10.5	11.1	4.05
Th	1.00	1.40	3.04	0.246	0.373	0.382	0.508	0.511	1.13	1.15	0.953	3.53	0.300
U	0.435	0.627	1.213	0.138	0.191	0.177	0.243	0.241	0.536	0.545	0.441	1.169	0.142

Sample	M3-04-08	M3-05-08	M3-07-08	M3-08-08	CM-29	CM-193	CM-201b	CM-210	CM-211	KR1-2	CM-9a	M3-09-08	M3-01-08
Center	Mutn. III	Mutn. III	Mutn. III	Mutn. III	Mutn. III	Mutn. III	Mutn. III	Mutn. III	Mutn. III	Mutn. III	Mutn. III	Mutn. III	Mutn. III
Map #	27	28	29	30	31	32	33	34	35	36	37	38	39
Location	52.4808	52.4802	52.4764	52.4601						52.4711		52.4634	52.4759
	158.1266	158.1255	158.1020	158.1616						158.1739		158.1676	158.1022
SiO_2	51.68	51.34	50.20	49.49	50.43	53.64	52.25	50.22	49.39	56.95	53.65	59.29	64.09
TiO_2	1.15	1.15	1.11	0.60	1.16	1.17	0.98	0.93	0.82	0.96	0.80	0.85	1.27
Al_2O_3	18.44	18.43	19.66	22.95	18.07	18.07	20.50	17.83	17.81	16.49	19.31	18.15	16.00
FeO[a]	11.03	11.24	10.24	7.23	10.07	9.20	8.01	9.16	9.69	8.90	7.95	6.60	5.65
MnO	0.20	0.21	0.18	0.13	0.15	0.18	0.25	0.11	0.18	0.16	0.14	0.13	0.21
MgO	4.51	4.70	4.23	4.46	5.81	4.93	4.51	8.24	8.50	4.27	5.47	2.18	1.55
CaO	9.29	9.30	10.69	12.58	11.04	8.87	10.64	10.96	10.74	7.84	9.33	7.29	3.35
Na_2O	3.17	3.08	2.95	2.19	2.65	2.94	2.06	2.07	2.28	2.82	2.53	3.68	4.93
K_2O	0.38	0.37	0.54	0.28	0.46	0.80	0.62	0.28	0.40	1.38	0.67	1.63	2.71
P_2O_5	0.15	0.17	0.20	0.09	0.15	0.19	0.18	0.22	0.19	0.23	0.15	0.21	0.25
Mg#	0.42	0.43	0.42	0.52	0.51	0.49	0.50	0.62	0.61	0.46	0.55	0.37	0.33
Rb	3.17	3.73	9.76	6.25	1.58	8.34	4.71	7.76	7.04	28.3	12.5	40.2	64.6
Sr	479	485	430	451	469	459	497	503	514	402	457	405	271
Y	22.0	15.2	30.8	20.3	25.0	36.9	23.0	23.6	23.6	30.1	24.9	35.2	54.8
Zr	47.3	49.0	75.6	57.3	53.0	88.0	58.6	72.5	70.5	141.6	79.2	189	408
Nb	1.06	1.14	1.78	1.09	1.02	1.99	1.32	2.02	1.93	3.08	1.54	3.76	12.30
Cs	0.149	0.270	0.558	0.501	0.124	0.439	0.317	0.429	0.359	1.75	0.803	2.51	2.39
Ba	165	168	209	174	164	302	198	232	223	406	262	540	1069
La	3.92	2.71	5.90	4.07	4.19	9.81	5.32	6.87	6.84	10.34	5.76	13.2	31.5
Ce	12.1	7.96	16.1	11.1	12.1	24.4	14.3	17.5	17.5	25.5	15.6	32.6	75.1
Pr	1.96	1.29	2.73	1.81	2.05	3.91	2.38	2.79	2.76	3.80	2.47	4.77	9.96
Nd	10.5	6.88	14.2	9.35	10.9	19.3	12.3	13.7	13.6	17.8	12.3	22.1	42.2
Sm	3.20	2.16	4.19	2.80	3.36	5.33	3.54	3.75	3.71	4.65	3.46	5.52	9.55
Eu	1.18	0.81	1.46	1.02	1.15	1.63	1.29	1.27	1.27	1.26	1.11	1.45	2.44
Gd	3.76	2.57	5.02	3.35	4.10	6.14	4.05	4.17	4.13	5.07	4.03	5.93	9.32
Tb	0.665	0.455	0.872	0.592	0.685	1.04	0.686	0.699	0.690	0.870	0.688	1.01	1.57
Dy	4.24	2.90	5.60	3.80	4.43	6.55	4.30	4.38	4.31	5.48	4.40	6.35	9.73
Ho	0.869	0.603	1.17	0.790	0.913	1.35	0.870	0.892	0.880	1.122	0.916	1.30	2.00
Er	2.49	1.71	3.34	2.25	2.55	3.89	2.48	2.50	2.49	3.20	2.59	3.75	5.79
Tm	0.373	0.258	0.500	0.340	0.384	0.574	0.370	0.367	0.364	0.479	0.399	0.565	0.902
Yb	2.43	1.71	3.28	2.25	2.49	3.81	2.45	2.42	2.38	3.19	2.60	3.78	6.08
Lu	0.365	0.258	0.496	0.332	0.390	0.584	0.375	0.365	0.357	0.478	0.413	0.571	0.940
Hf	1.53	1.56	2.26	1.74	1.67	2.55	1.71	2.02	1.95	3.96	2.35	5.23	9.61
Ta	0.058	0.061	0.106	0.070	0.060	0.116	0.073	0.114	0.109	0.213	0.101	0.265	0.745
Pb	3.99	4.33	4.67	4.37	3.64	6.50	4.51	4.27	3.97	9.20	5.52	10.2	17.9
Th	0.262	0.259	0.658	0.512	0.331	0.658	0.275	0.526	0.506	2.05	0.827	3.00	4.91
U	0.105	0.113	0.271	0.217	0.158	0.295	0.148	0.228	0.219	0.896	0.373	1.324	1.993

Sample	CM-8a	M4-01-08	CM-196	CM-206	CM-68	CM-61a	CM-63a	CM-67	CM-198	KR-1	CM-62
Center	Mutn. III	Mutn. IV	Mutn. IV	Mutn. IV	Mutn. IV	Mutn. IV	Mutn. IV	Mutn. IV	Mutn. IV	Mutn. IV	Mutn. IV
Map #	40	41	42	43	44	45	46	47	48	49	50
Location		52.4607									
		158.1617									
SiO_2	69.60	53.19	49.60	51.97	50.95	50.19	50.30	48.97	50.14	54.94	54.24
TiO_2	0.63	0.99	0.85	1.13	0.78	1.06	1.01	1.00	0.93	0.91	1.00

(*continued on next page*)

Table 1 (*continued*)

Sample	CM-8a	M4-01-08	CM-196	CM-206	CM-68	CM-61a	CM-63a	CM-67	CM-198	KR-1	CM-62
Center	Mutn. III	Mutn. IV	Mutn. IV	Mutn. IV	Mutn. IV	Mutn. IV	Mutn. IV	Mutn. IV	Mutn. IV	Mutn. IV	Mutn. IV
Map #	40	41	42	43	44	45	46	47	48	49	50
Location		52.4607 158.1617									
Al_2O_3	14.65	19.37	19.22	18.31	20.94	19.97	19.15	20.25	18.12	16.93	17.44
FeO[a]	3.66	9.97	9.99	9.27	7.94	9.63	9.45	10.05	9.66	9.16	8.67
MnO	0.10	0.16	0.18	0.20	0.18	0.21	0.14	0.18	0.19	0.16	0.15
MgO	0.75	3.93	6.27	5.39	5.15	5.08	6.25	5.40	7.22	5.26	5.02
CaO	3.10	8.85	10.90	10.40	11.17	10.73	10.41	10.73	10.84	8.96	8.99
Na_2O	4.19	2.82	2.54	2.54	2.25	2.45	2.51	2.71	2.27	2.65	3.10
K_2O	3.19	0.55	0.29	0.61	0.55	0.42	0.55	0.55	0.49	0.85	1.20
P_2O_5	0.12	0.17	0.16	0.17	0.10	0.25	0.23	0.16	0.14	0.18	0.18
Mg#	0.27	0.41	0.53	0.51	0.54	0.48	0.54	0.49	0.57	0.51	0.51
Rb	53.6	9.67	2.82	5.75	2.98	4.76	6.53	4.91	3.83	17.0	16.8
Sr	177	471	474	520	437	501	498	472	461	427	432
Y	48.2	28.7	21.4	24.9	15.5	21.8	26.2	25.4	21.5	24.6	25.3
Zr	321	70.0	56.8	65.2	43.5	53.8	78.4	58.6	62.2	97	102
Nb	5.63	1.55	1.38	1.45	1.05	1.17	1.73	1.08	1.43	2.03	2.08
Cs	3.72	0.714	0.124	0.378	0.323	0.423	0.471	0.435	0.408	1.08	1.18
Ba	900	222	187	204	125	161	223	169	169	282	307
La	16.6	6.07	5.08	5.64	3.14	4.08	6.66	4.37	4.87	7.1	7.42
Ce	44.7	16.0	13.4	14.8	8.8	11.7	18.4	12.8	12.9	17.9	19.5
Pr	6.23	2.58	2.19	2.43	1.45	1.95	2.89	2.19	2.11	2.75	2.96
Nd	28.1	13.3	11.0	12.4	7.36	10.1	14.4	11.5	10.7	13.4	14.2
Sm	7.01	3.92	3.13	3.55	2.16	2.99	3.95	3.43	3.10	3.69	3.79
Eu	1.37	1.38	1.14	1.27	0.77	1.08	1.31	1.22	1.13	1.14	1.12
Gd	7.53	4.73	3.65	4.18	2.58	3.60	4.44	4.18	3.64	4.15	4.31
Tb	1.29	0.811	0.623	0.710	0.437	0.606	0.758	0.721	0.628	0.713	0.710
Dy	8.30	5.21	3.95	4.51	2.84	3.96	4.74	4.62	3.96	4.49	4.52
Ho	1.73	1.08	0.806	0.924	0.584	0.818	0.965	0.962	0.811	0.92	0.920
Er	5.04	3.07	2.30	2.64	1.66	2.31	2.71	2.71	2.31	2.64	2.61
Tm	0.793	0.459	0.345	0.388	0.247	0.345	0.407	0.406	0.339	0.390	0.394
Yb	5.32	3.04	2.24	2.57	1.63	2.26	2.68	2.67	2.24	2.57	2.58
Lu	0.844	0.456	0.342	0.394	0.259	0.357	0.413	0.417	0.341	0.389	0.409
Hf	8.93	2.08	1.64	1.89	1.31	1.65	2.23	1.85	1.76	2.73	2.91
Ta	0.410	0.093	0.071	0.081	0.055	0.064	0.095	0.063	0.079	0.135	0.136
Pb	18.1	5.16	3.17	5.20	2.99	3.87	4.93	4.24	3.77	6.17	6.91
Th	4.79	0.501	0.286	0.389	0.308	0.313	0.421	0.274	0.308	1.22	1.36
U	1.889	0.236	0.132	0.190	0.136	0.144	0.198	0.149	0.161	0.525	0.555

[a] Major elements are reported on an anhydrous basis with totals recalculated to 100%. Map # refers to sample locations shown in Fig. 2. Mg-number (Mg#) is molar Mg/(Mg + Fe) using the total Fe content.

dominantly basalt (Selyangin, 1993). This is like most Kamchatka volcanoes, which are composed mainly of basalt and basaltic andesite (i.e., 50–85% of the total mapped rock volume; Volynets, 1994; Ponomareva et al., 2007). Mutnovsky lavas have relatively low SiO_2, Na_2O and K_2O and somewhat higher TiO_2, CaO and Al_2O_3 compared to Quaternary-age volcanic rocks throughout Kamchatka (relative to

Table 2
Sr, Nd, Hf, Pb and O isotope results for Mutnovsky samples.[a]

Field ID	$^{87}Sr/^{86}Sr$	$^{143}Nd/^{144}Nd$	ε_{Nd} [b]	$^{176}Hf/^{177}Hf$	2σ[c]	ε_{Hf}[a]	$^{206}Pb/^{204}Pb$	2σ[c]	$^{207}Pb/^{204}Pb$	2σ[c]	$^{208}Pb/^{204}Pb$	2σ[c]	$\delta^{18}O$	2σ
CM-97a	0.703387	0.513108	9.3	0.283226	±4	15.6	18.3589	±9	15.5055	±8	38.1292	±46		
M1-02-08	0.703384	0.513053	8.3	0.283224	±4	15.5	18.3670	±8	15.5087	±9	38.1416	±27		
CM-47	0.703380	0.513060	8.4	0.283219	±5	15.3	18.3572	±8	15.5053	±8	38.1327	±22		
CM-156	0.703355	0.513089	9.0	0.283236	±6	15.9	18.3923	±74	15.5183	±94	38.1855	±310		
CM-155	0.703361	0.513071	8.6	0.283229	±5	15.7	18.3696	±9	15.5110	±6	38.1550	±26		
CM-113	0.703358	0.513077	8.7	0.283224	±4	15.5	18.3691	±6	15.5068	±6	38.1376	±21		
M3-08-08	0.703335	0.513101	9.2	0.283225	±5	15.6	18.3730	±12	15.5074	±13	38.1492	±59		
M3-09-08	0.703371	0.513146	10.1	0.283221	±4	15.4	18.3647	±7	15.5135	±6	38.1585	±41		
CM-8a	0.703342	0.513083	8.8	0.283222	±5	15.5	18.3647	±9	15.5124	±8	38.1539	±23		
CM-196							18.3727	±30	15.5069	±20	38.1417	±130		
CM-206	0.703354	–		0.283229	±4	15.7	18.3669	±8	15.5031	±9	38.1335	±32		
CM-68	0.703346	0.513079	8.8	0.283232	±5	15.8							5.340	±21
CM-62	0.703340	0.513077	8.7	0.283220	±4	15.4							5.120	±50
CM-61a													5.295	±35
CM-63a													5.505	±15
CM-67													5.285	±55
CM-198													5.435	±25

Multiple standard runs.
[a] Sr, Nd, Hf and Pb are whole-rock lavas compositions. Oxygen isotopes are for olivine mineral separates.
[b] ε_{Hf} and ε_{Nd} are calculated using chondritic values of $^{176}Hf/^{177}Hf = 0.282785$ and $^{143}Nd/^{144}Nd = 0.512630$ (Bouvier et al., 2008).
[c] Within-run uncertainties for Pb and Hf are 2σ expressed as variation in the last decimal place. Uncertainty estimates are ±20 ppm for $^{87}Sr/^{86}Sr$ and ±0.25 ε_{Nd} based on multiple standard runs

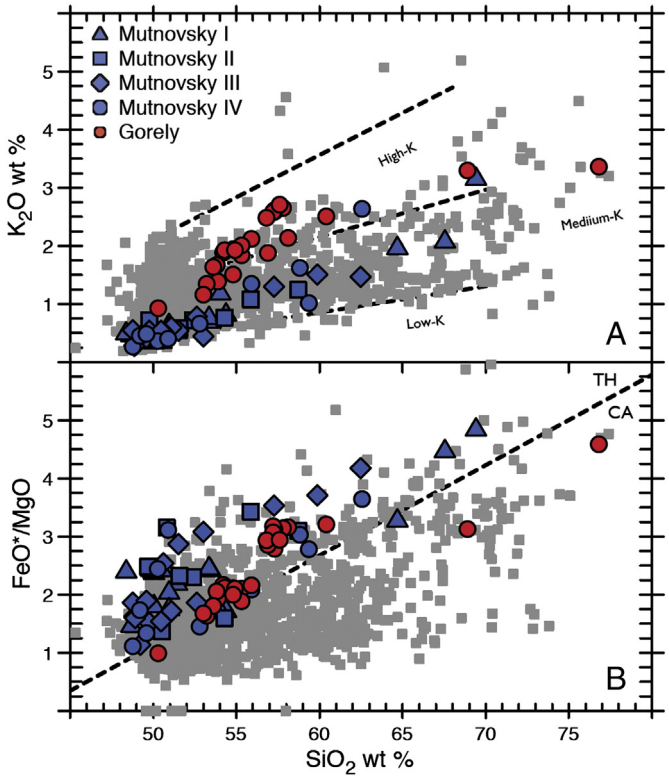

Fig. 3. Graphs of K_2O and FeO/MgO versus SiO_2 for Mutnovsky and Gorely lavas, compared with published data for all Kamchatka volcanoes. Dashed lines in 3A separating the low, medium and high-K fields are from Gill (1981). The dashed line in 3B separating the tholeiitic (TH) and calc-alkaline (CA) fields is from Miyashiro (1974). Gorely data are from Duggen et al. (2007). Gray symbols are published, volcanic rock compositions from Kamchatka volcanoes. These data are from sources cited below. Additional sources are cited in Portnyagin et al. (2007a, 2007b). (Fedotov and Markhinin, 1983; Fedotov and Masurenkov, 1991; Kersting and Arculus, 1994, 1995; Braitseva et al., 1996; Hochstaedter et al., 1996; Kepezhinskas et al., 1997; O.N. Volynets et al., 1997, 1999, 2000; Ozerov et al. 1997; Turner et al., 1998; Alves et al., 1999; Pineau et al., 1999; Dorendorf et al., 2000a,b; Ozerov, 2000; Churikova et al., 2001; Ishikawa et al., 2001; Bindeman et al., 2004; Izbekov et al., 2004; Bindeman et al., 2005; Portnyagin et al., 2005; Dirksen et al., 2006; Duggen et al., 2007; Ponomareva et al., 2007; Portnyagin et al., 2007a,b; Turner et al., 2007; Ivanov et al., 2008; Grib et al., 2009; A.O. Volynets et al., 2010; Bindeman et al., 2010; Bryant et al., 2011; Ferlito, 2011; Gorbach & Portnyagin, 2011a,b; Churikova et al., 2012; Viccaro et al., 2012; Almeev et al., 2013).

MgO — Fig. 4). Low K_2O is a distinctive aspect of Mutnovsky basalts and basaltic andesites (mean $K_2O = 0.52 \pm 0.23$ %, n = 41, $\pm 1\sigma$) compared to lavas throughout Kamchatka with similar MgO contents of 4.0–8.5% (mean $K_2O = 1.15 \pm 0.38$ wt.%, n = 1005, $\pm 1\sigma$, Fig. 4B). Total iron at Mutnovsky (FeO*) is variable, and includes samples at 4–6% MgO that show both Fe-enrichment and depletion compared to more primitive samples with 7–9% MgO (Fig. 4F). Lavas from nearby Gorely Volcano, which is located behind the volcanic front, approximately 15 km west of Mutnovsky, have higher average SiO_2, Na_2O and K_2O and lower average FeO*. The compositional contrast between Mutnovsky and Gorely lavas is particularly clear for K_2O and P_2O_5 (Fig. 4B,H).

Trace element compositions of Mutnovsky samples (illustrated in Figs. 5–8), are similar for all centers, with the exception of dacites from Mutnovsky II. Consistent with their low K_2O contents, Mutnovsky basalts and basaltic andesites have low concentrations of strongly incompatible elements. This is evident for Ba, Th, Ce and Nb, which are present in relatively low concentrations in Mutnovsky mafic lavas compared to other Kamchatka samples with similar SiO_2 and MgO (Fig. 7). Mutnovsky basalts and basaltic andesites are depleted in the light REEs, have chondrite-normalized La/Sm frequently <1 (Fig. 5), and relatively high abundances of heavy REEs (Fig. 7B). In contrast, enrichments in Ba in Mutnovsky basalts and basaltic andesites are relatively high (Ba/La = 20–60; Ba/Th = 300–900) as is commonly seen in mafic lavas from other Kamchatka volcanoes (Fig. 8A, E). Abundances of high field strength elements (HFSEs) compared to other, similarly incompatible trace elements (e.g., Ta/La, Hf/Nd) are low in Mutnovsky lavas compared to MORB (Fig. 6) and so are typical of arc lavas worldwide. Concentrations of incompatible trace elements generally increase with increasing SiO_2 and decreasing MgO (Fig. 7). Ratios among incompatible elements are similar for Mutnovsky basalts and basaltic andesites (Fig. 8) but variability of both trace element concentrations and ratios is significantly greater for Mutnovsky andesites and dacites compared to more mafic lavas (Fig. 7).

Dacites from Mutnovsky I and II have trace element patterns that contrast with more mafic rocks from those centers (Table 1). The Mutnovsky I and II dacites are more depleted in the middle and heavy REEs relative to Mutnovsky samples with lower SiO_2 and higher MgO (Figs. 5, 7). This pattern is particularly clear for sample CM-113 from Mutnovsky II (Table 1), which has abundances of REEs that are mostly below those of the associated basalts and basaltic andesites (Fig. 5). Concentrations of Ba, Th and other strongly incompatible trace elements, including Hf and Zr in this depleted dacite is higher than in the more mafic lavas (Fig. 6A).

4.2. Isotopes

New Sr, Nd, Pb and Hf isotope data for Mutnovsky samples are presented in Table 2 and illustrated in Figs. 9–11. Data from Mutnovsky and Gorely volcanoes from Duggen et al. (2007) and published data from all Kamchatka volcanoes are also plotted. Like most Kamchatka lavas, the Mutnovsky samples have relatively radiogenic Nd isotopes (ε_{Nd} ~ 8.0–9.5), similar to the non-radiogenic end of the Pacific MORB field, but offset from Pacific MORB toward more radiogenic Sr, with $^{87}Sr/^{86}Sr$ ~ 0.7033 (Fig. 9). Mutnovsky samples are slightly more radiogenic in both Nd and Sr isotopes compared to samples from neighboring Gorely volcano. Hafnium isotopes for Mutnovsky samples measured for this study, fall within an even more narrow range than Nd (ε_{Hf} = 15.3–15.9). As a group, the Mutnovsky and Gorely lavas form a tight cluster with relatively radiogenic Hf compared to Nd, near the center of the terrestrial array, with more radiogenic Hf compared to both Pacific and Indian MORB (Fig. 10). For Pb isotopes, the Mutnovsky and Gorely samples define a narrow range of compositions at the radiogenic end of the Kamchatka array in Pb isotope space, with $^{206}Pb/^{204}Pb$ ~ 18.36 and $^{207}Pb/^{204}Pb$ ~ 15.51 (Fig. 11). There are no systematic isotopic differences across eruptive centers or rock types (Fig. 12). The $\delta^{18}O$ of olivine phenocrysts from Mutnovsky IV range from 5.12 ± 0.050 to 5.505 ± 0.015 (Table 2). The range of published $\delta^{18}O$ from Kamchatka is from +4.1 to +10.8‰, with approximately half of all Kamchatka samples yielding primitive mantle $\delta^{18}O$ values (Volynets, 1994; Bindeman et al., 2004).

5. Discussion

5.1. Evolution of basalts, basaltic andesites and andesites

The Sr, Nd, Pb and Hf isotopic signatures are consistent with all Mutnovsky samples sharing a common source. We used the least-squares program XLFRAC (Stormer and Nicholls, 1978) to model the major element and REE evolution of Mutnovsky basaltic andesites and andesites. The model results for major elements indicate that fractionation of variable amounts of olivine and clinopyroxene, coupled with minor assimilation of a high-silica compositions (e.g., dacite) can produce basaltic andesites from a parental basalt composition. Table 3 presents AFC model results using the compositions of basalt CM-48 and dacite CM-47 to produce a basaltic andesite The model results indicate that 20% FC of 6% olivine, 3% clinopyroxene and 91% plagioclase from basalt CM-48, coupled with assimilation of dacite CM-47 in the ratio 1:9 (dacite/basalt) produce a basaltic andesite composition that is similar to basaltic andesite M1-06-08 (Table 3). The sum of the squares of residuals is 1.63 (Table 3). The fractionating assemblage clinopyroxene,

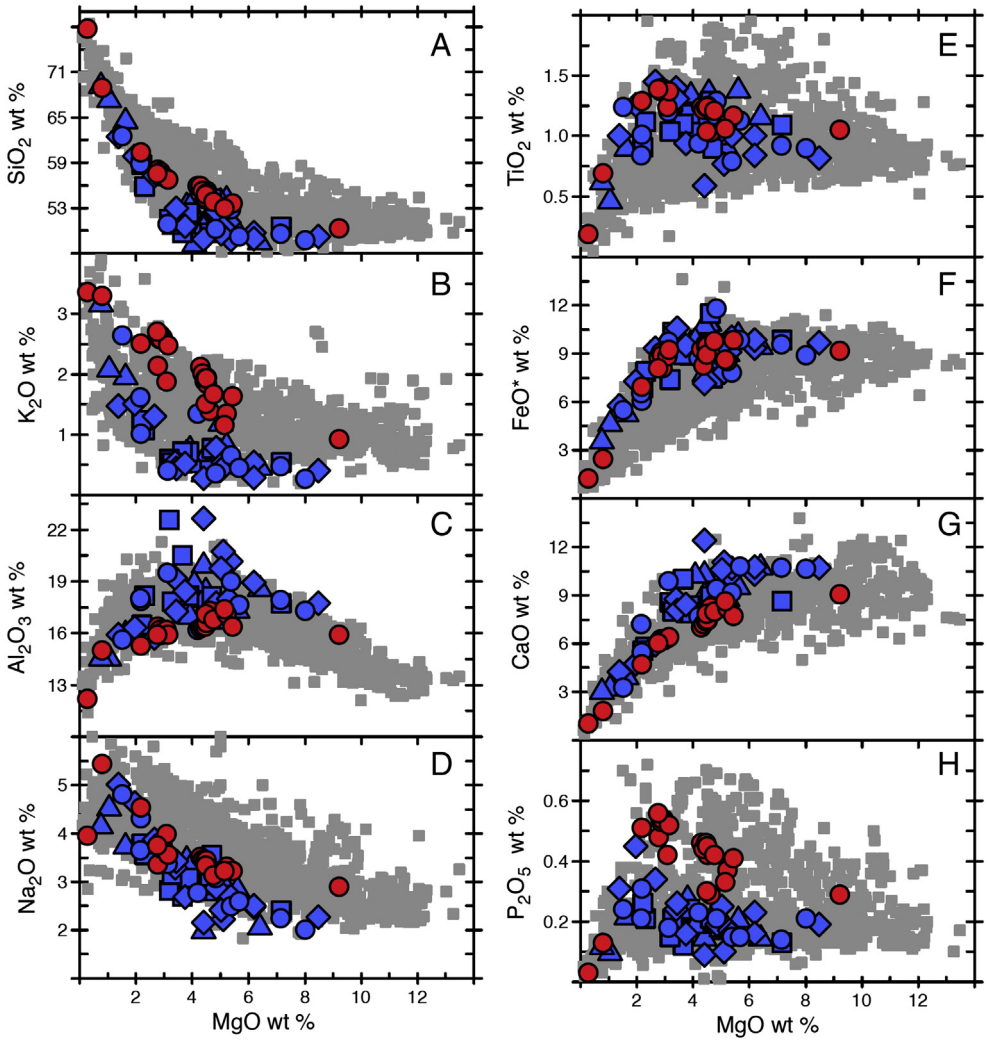

Fig. 4. Major element Harker diagrams for Mutnovsky and Gorely samples, compared with published data for Kamchatka volcanic rocks. Symbols and data sources are the same as in Fig. 3.

orthopyroxene and plagioclase is consistent with petrographic observations (Electronic Appendix **A**). The XLFRAC results indicate that a model andesite similar to andesite CM-24 can be produced by 11% FC of 100% plagioclase from basaltic andesite M1-06-08. The sum of squares of residuals is 1.212 (Table 3).

The evolution of the REE abundances was modeled by using the IgPet software program (Carr, 2007) and the partition coefficients provided in Table 4 and reported in Wanless et al. (2010), which were varied appropriately for the range of compositions modeled. These model results are presented in Fig. 13. The model results indicate that the REE compositions of a basaltic andesite such as M1-06-08 can be generated by 15% FC of 6% olivine, 3% clinopyroxene and 91% plagioclase from basalt CM-48, combined with assimilation of dacite CM-47 with R (mass assimilated/mass fractionated) = 0.1 (Fig. 13a). Further, an andesite similar to composition CM-24 can be generated by 8% FC of 100% plagioclase, combined with assimilation of dacite CM-47 with R = 0.4 (Fig. 13b). These model results for the REE abundances are consistent with the results of the major element models (Table 3). We highlight that andesites are volumetrically minor compared with more mafic magmas; hence, the models results for the required % FC % are plausible. Our results are also consistent with other geochemical studies of arc magmas that invoke and model FC to explain evolved compositions (e.g., Conrad and Kay, 1984; Grove et al., 2005).

5.2. Origin of Mutnovsky I and II dacites

Dacites that erupted from Mutnovsky I and II have trace element abundances, notably the REE, that are depleted relative to more mafic lavas from the same eruptive centers (Fig. 5). If the dacites were produced by FC of more mafic magmas, this requires a fractionating phase that caused the REE concentrations to decrease during FC. Several studies suggested that fractionation of amphibole causes a decrease of the REE abundances of a silicate liquid (Kay and Kay, 1985; Romick et al., 1992; Davidson et al., 2007; Hidalgo and Rooney, 2010; Rooney et al., 2010). The fractionation of amphibole imparts a unique MREE-depleted signature, similar to the depleted MREE pattern observed for the dacites at Mutnovsky I and II (Fig. 5). Model FC results indicate that the fractionation of 1 to 80 modal % amphibole from an andesitic melt, using a wide range of amphibole / melt partition coefficients from the Geochemical Earth Reference Model (GERM, earthref.org) database and Hidalgo and Rooney (2010), cannot reproduce the Mutnovsky I and II dacite compositions by amphibole FC of any melt composition less evolved than dacite. Thus, we conclude that the Mutnovsky dacitic magmas are not the product of FC of a more mafic magma. Additional plausible scenarios for the origin of the dacites include partial melting of subducting oceanic crust, and partial melting of underplated amphibole-bearing basaltic rock, which formed from

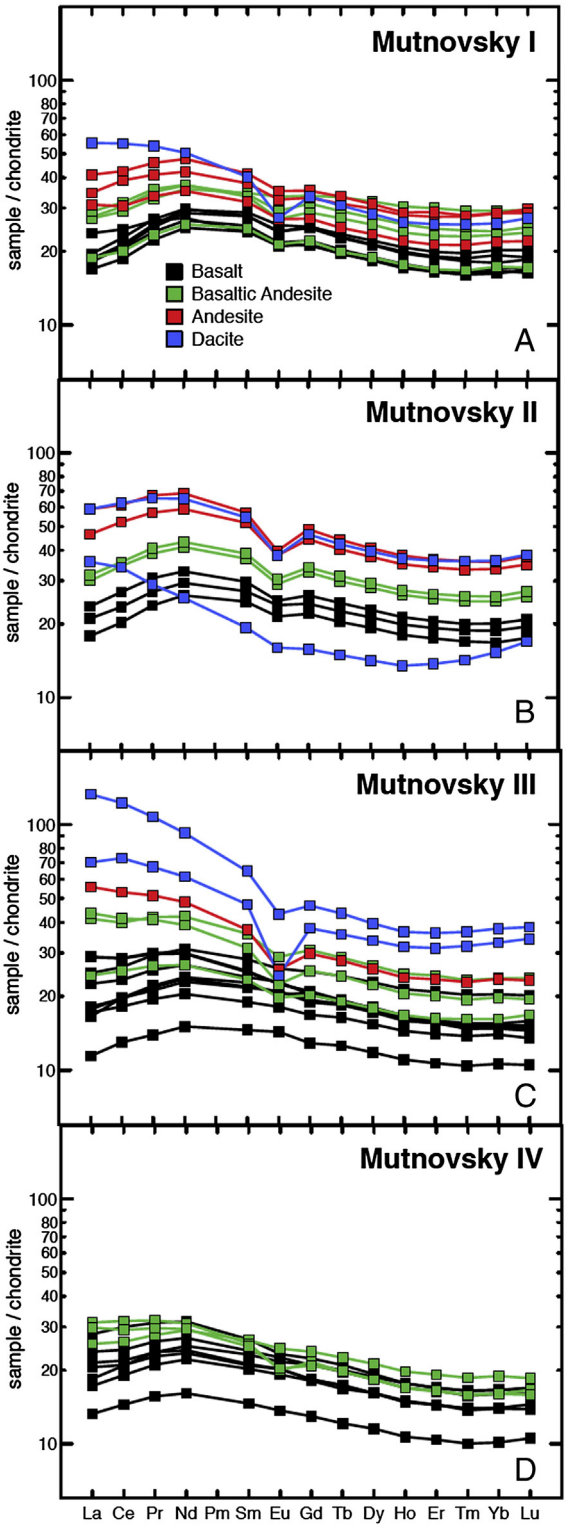

Fig. 5. Rare earth element abundances for Mutnovsky 1–IV volcanic rocks, normalized to chondritic values of Sun and McDonough (1989).

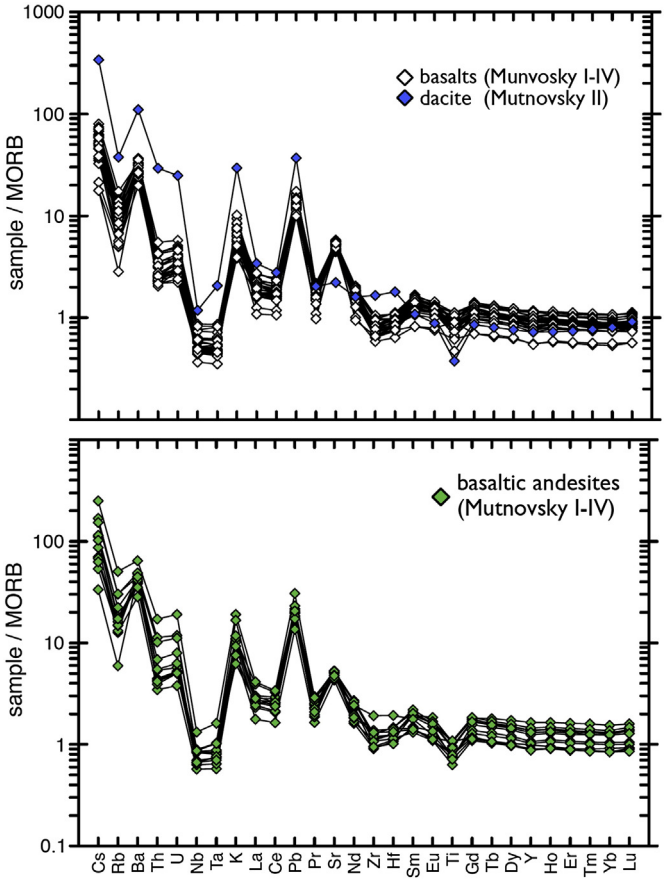

Fig. 6. Trace element abundances for Mutnovsky basalt and basaltic andesite samples of all ages, compared to dacite from Mutnovsky II, which has low abundances of rare earth elements. Values are normalized to normal mid-ocean ridge basalt values of Sun and McDonough (1989).

the crystallization of previously intruded hydrous basaltic magmas within the Mutnovsky plumbing system.

Most Cenozoic-age volcanic rocks with trace element patterns interpreted to have formed by melting of subducted oceanic crust are calc-alkaline andesites and dacites with fractionated trace element patterns (e.g., La/Yb > 20, Sr/Y > 40) indicating a significant role for residual garnet (e.g., Adak; Baja; Costa Rica-Panama (Abratis and Wörner, 2001); Patagonia (Goring and Kay, 2001); Ecuador (Bourdon et al., 2002); Japan (Morris, 1995)). Less commonly, they are primitive, high-Mg# andesites with less strongly fractionated trace element patterns that match more closely those of average arc rocks (e.g., Setouchi (Shimoda et al., 1998); Piip (Yogodzinski et al., 1994); Shisheisky (Bryant et al., 2011)). Dacites sampled from Mutnovsky I and II are highly evolved magmas, with Mg#s < 30 (Table 1), with relatively unfractionated trace element patterns (e.g., Sr/Y of 12.5 and 20.1), and have low abundances of REE relative to published compositions of slab melts. Experimental data indicate that melting of subducted ocean crust will produce partial melts that have high SiO_2, low MgO, and a low Mg#. Interaction of such slab melts with the overlying mantle peridotite will cause a shift toward lower silica and higher Mg# (Yu et al., 2014). The absence of a high-Mg#, highly calc-alkaline composition for the Mutnovsky dacites (Table 1) therefore argues against this interpretation.

The second model to produce dacitic magma invokes partial melting of underplated amphibole-bearing basaltic rock in the middle- to deep-crust (cf. Beard and Lofgren, 1989; Beard and Lofgren, 1991; Rapp et al., 1991; Coleman et al., 1992; Tepper et al., 1993; Rapp and Watson, 1995; Lange and Carmichael, 1996; Borg and Clynne, 1998). Partial melting experiments demonstrate that small to moderate degree partial melts of underplated amphibole-bearing basaltic rock can plausibly produce dacitic magma (e.g., Beard and Lofgren, 1989; Beard and Lofgren, 1991; Rapp et al., 1991; Rushmer, 1991; Rapp and Watson, 1995). The REE patterns of the Mutnovsky I and II dacites are plotted in Fig. 13a, together with the REE patterns for silicate melts that were produced by vapor-absent partial melting experiments (Rapp et al., 1991; Rapp and Watson, 1995) of amphibole-bearing basaltic rock at 8 kbar, and 900 and 1000 °C. The partial melting experiments produced a silicate melt

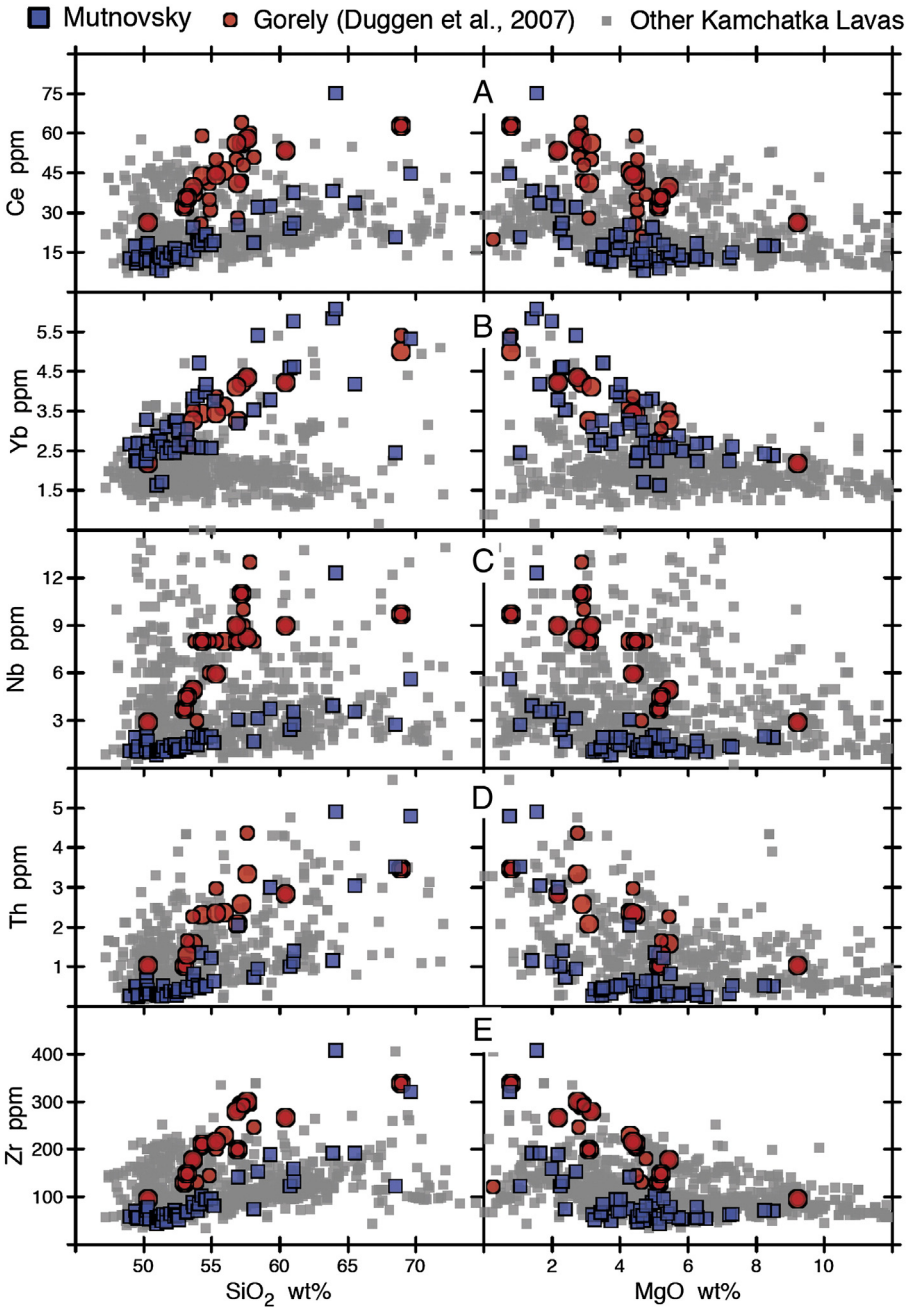

Fig. 7. Trace element abundances for Ce, Yb, Nb, Th and Zr plotted against SiO_2 and MgO for Mutnovsky and Gorely volcanic rocks. Symbols are the same as in Fig. 4. Other Kamchatka data are from sources cited in the caption of Fig. 3.

that is dacitic to rhyodacitic in composition, with a restite that consists of plagioclase, amphibole and orthopyroxene. These experimental results indicate that partial melting of amphibole-bearing basaltic rock leaves an amphibole-bearing residue in the middle crust. The residual amphibole sequesters the REE, most notably the middle and heavy REE, and results in a higher-SiO_2 (i.e., dacitic) magma. Published experimental data (Rapp et al., 1991; Rapp and Watson, 1995) indicate that at pressures equivalent to mid-crustal depths (i.e., 8 kbar), garnet is absent from the restite, an empirical finding consistent with decreasing trends of La/Yb and Dy/Yb with increasing SiO_2 measured in Mutnovsky magmas (cf. Kay, 1978; Yogodzinski et al., 1995). This trend is opposite of what is expected if garnet is a restitic phase. As indicated by the experimental data plotted in Fig. 14a, increasing the temperature of partial melting of amphibole-bearing basaltic rock, at 8 kbar, from 900 to 1000 °C results in partial melt that has higher total REE abundances (e.g., La and Lu are a factor of 5 and 2 higher, respectively). This temperature increase also increases the ratio of La/Lu from approximately 2 at 900 °C to 5 at 1000 °C. Fig. 14b shows the model results for REE batch melting of amphibole-bearing basaltic rock that contains 60% cpx, 10% ol, and 30% hornblende. The model results indicate that batch melting of between 20 and 25% of amphibole-bearing basaltic rock reproduces the REE signature of Mutnovsky dacites. We used basalt M1-04-08 as a proxy for an amphibolite source, assuming that the underplated basaltic rock intruded during an earlier episode of activity. This assumption is consistent with overlapping Sr, Nd, Pb and Hf isotopic compositions of Mutnovsky dacites and basalts (Table 2) and also made in other studies (e.g., Turner et al., 2012). The batch melting model is more responsive to the modal abundance of hornblende and is relatively insensitive to the abundances of olivine and clinopyroxene. We interpret the batch melting model results (Fig. 14b) to indicate that the Mutnovsky dacites

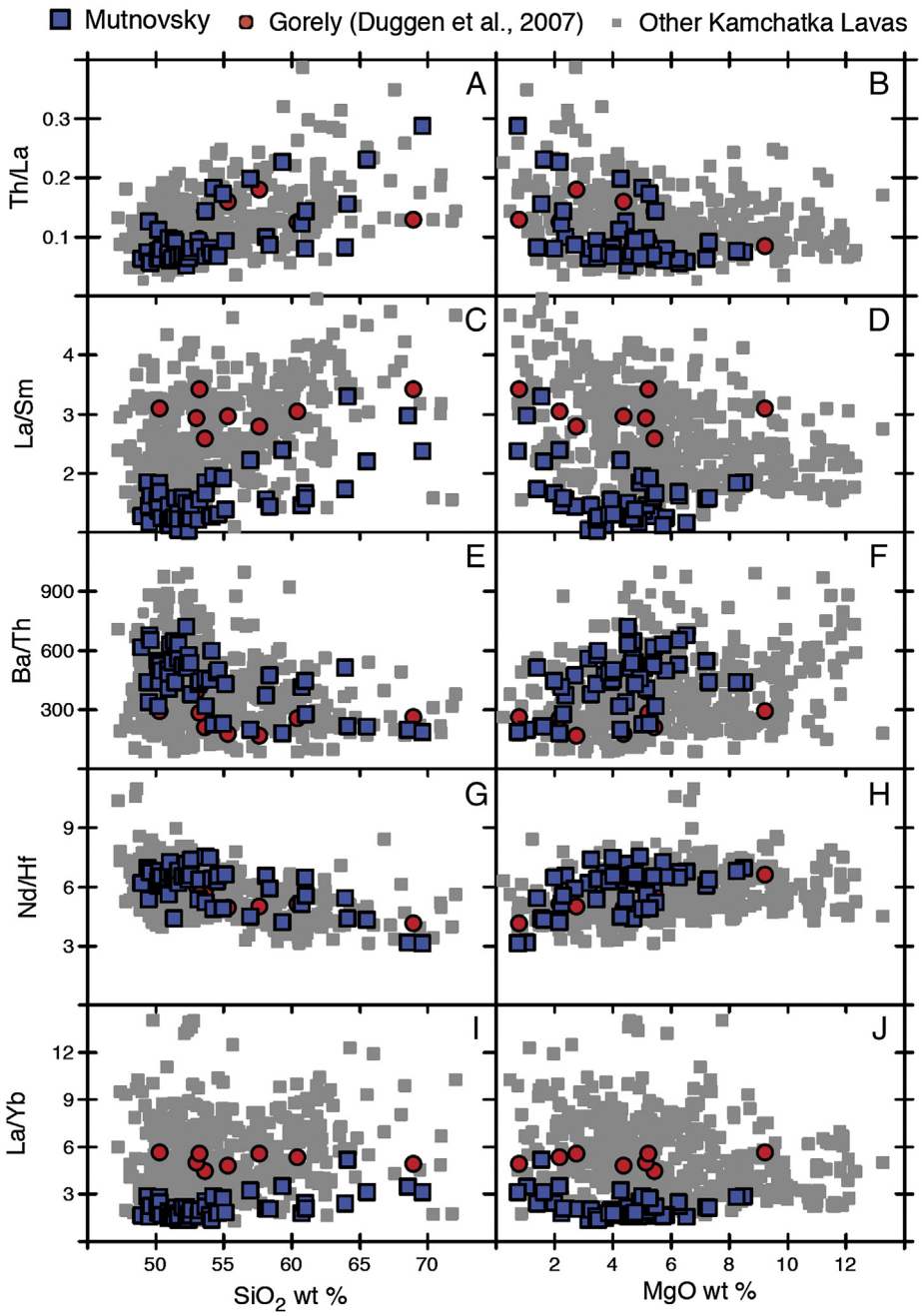

Fig. 8. Trace element ratios plotted against SiO_2 and MgO for Mutnovsky and Gorely volcanic rocks. Symbols are the same as in Fig. 4. Other Kamchatka data are from sources cited in the caption of Fig. 3.

formed via partial melting of mid-crustal, amphibole-bearing basaltic rock. This interpretation is consistent with other studies that investigated the evolution of chemically evolved silicate magmas in arc environments (e.g., Coleman et al., 1992; Atherton and Petford, 1993; Tepper et al., 1993; Lange and Carmichael, 1996; Petford and Atherton, 1996; Borg and Clynne, 1998; Petford and Gallagher, 2001) and experimental studies that reported the production of broadly dacitic magma during vapor-absent partial melting of underplated amphibole-bearing basalt (Rapp et al., 1991; Rapp and Watson, 1995).

5.3. The source of Mutnovsky, Gorely and other Kamchatka lavas

Contrasting compositions of Mutnovsky and Gorely lavas provide a classic example of the K–h relationship of Dickinson and Hatherton (1967), wherein potassium concentrations of arc lavas (K) are observed to increase across the arc, with increasing depth to the Benioff zone (h). This pattern is reflected in higher concentrations of K_2O (Fig. 3A) and other incompatible trace elements in Gorely lavas compared to Mutnovky (Fig. 7; Duggen et al., 2007). Similar isotopic compositions for samples from both volcanoes, in particular with respect to Pb isotopes (Fig. 10), indicate that much of the cross-arc increase in K_2O and other incompatible element concentrations is probably produced by a somewhat lower degree of partial melting below Gorely compared to Mutnovsky (cf. Duggen et al., 2007). This is a widespread and long-standing interpretation of the K–h relationship, which has been recognized especially in northeast Japan (Nakamura et al., 1985; Sakuyama and Nesbitt, 1986; Shibata and Nakamura, 1997; Kimura and Yoshida, 2006), the Kurile arc (Ryan et al., 1995; Ishikawa and Tera, 1997; Bindeman and Bailey, 1999), and in the Isu–Bonin–Mariana arc (Stern et al., 1993; Kimura et al., 2010; Tollstrup et al., 2010). However, some

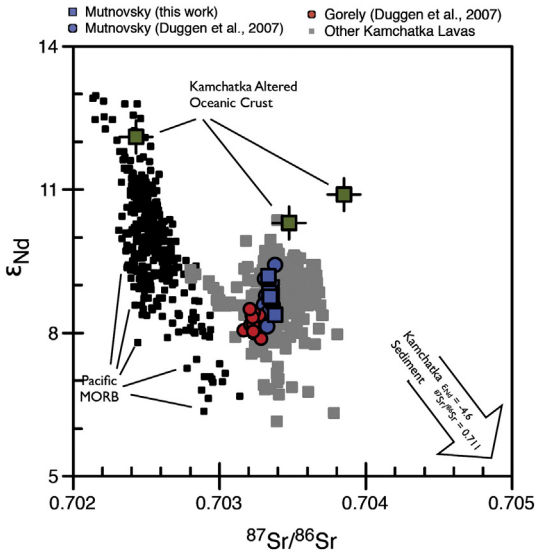

Fig. 9. Neodymium and Sr isotopic compositions for Mutnovsky and Gorely samples compared to Pacific MORB and other Kamchatka volcanic rocks. Other Kamchatka data are from sources cited in the caption of Fig. 3. Pacific MORB data are from these sources (Macdougall and Lugmair, 1986; Newsom et al., 1986; Hegner and Tatsumoto, 1987; Ito et al., 1987; Klein et al., 1988; Bach et al., 1994; Mahoney et al., 1994; Castillo et al., 1998; Niu et al., 1999; Regelous et al., 1999; Vlastélic et al., 1999; Wendt et al., 1999; Castillo et al., 2000; Chauvel and Blichert-Toft, 2001; Niu et al., 2002; Sims et al., 2002a, b; Davis et al., 2008; Hahm et al., 2009; Hamelin et al., 2010; Waters et al., 2011).

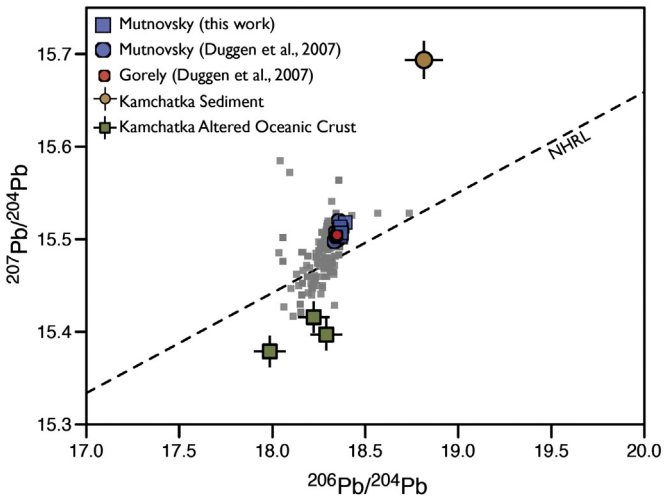

Fig. 11. Lead isotopic compositions ($^{206}Pb/^{204}Pb$ versus $^{207}Pb/^{204}Pb$) for Mutnovsky and Gorely samples compared to Kamchatka sediment from Plank and Langmuir (1998), and Kamchatka altered oceanic crust from Duggen et al. (2007). Other Kamchatka data are from sources cited in the caption of Fig. 3.

cross-arc changes in trace element ratios from Mutnovsky to Gorely are coupled to isotopic differences. This is evident for La/Yb, which is somewhat higher in Gorely samples, which have slightly more radiogenic Hf and Nd, compared to Mutnovsky (Fig. 15). These relationships indicate that cross-arc changes reflect at least modest changes in the source mixture, as well as changes in the degree of melting, as shown by Duggen et al. (2007). The exact nature of the source change is not clear though, because the patterns are not consistent with simple addition/subtraction of depleted mantle and subducted sediment components. This is evident from the Sr, Hf and Nd isotopes, which are all slightly less radiogenic at Goreley compared to Mutnovsky (Fig. 12). This pattern cannot be explained by a gain or loss of sediment from the source. This point is underscored by the Pb isotopes, which should be sensitive to changes in sediment, which is rich in Pb (13.8 ppm Pb in the bulk sediment package for Kamchatka — Plank, 2014), but which are effectively the same in Mutnovsky and Gorely samples (Fig. 11).

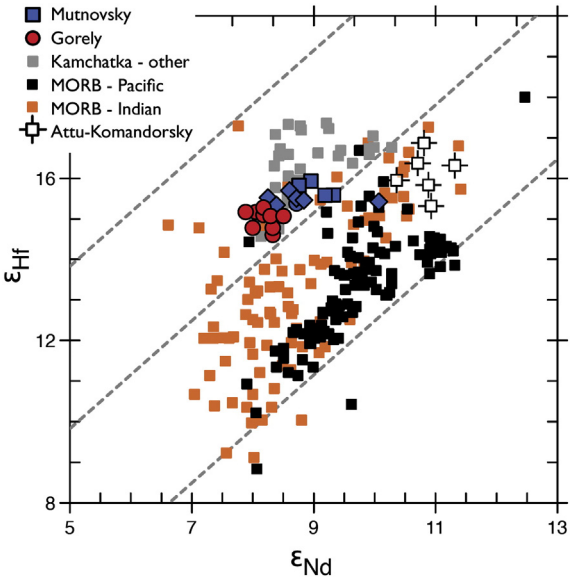

Fig. 10. Hafnium and Nd isotopic compositions for Mutnovsky and Gorely samples compared to Pacific and Indian MORB and other Kamchatka and western Aleutian volcanic rocks. Other Kamchatka and Aleutian data are from Münker et al. (2001), Duggen et al. (2007) and Yogodzinski et al. (2001). Pacific and Indian MORB data are from the following sources (Salters and Hart, 1991; Pyle et al., 1992; Salters, 1996; Nowell et al., 1998; Salters and White, 1998,; Chauvel and Blichert-Toft, 2001; Kempton et al., 2002; Mahoney et al., 2002; Sims et al., 2002a,b; Hanan et al., 2004; Janney et al., 2005; Graham et al., 2006; Meyzen et al., 2007; Hamelin et al., 2011; Waters et al., 2011).

In the broader context, and compared to other Kamchatka lavas, Mutnovsky samples have distinctive compositions, with relatively low K and Ba (Figs. 3A, 4B, 7B), which is coupled to enrichments in Ba relative to less soluble trace elements, such La and Th (Fig. 8A, D). Relative Ba enrichments are particularly well expressed in Ba/Th, which is highly variable up to ~720 in Mutnovsky basalts and basaltic andesites (Fig. 8D). This is common in Kamchatka lavas, but not at Gorely, where Ba/Th is mostly <300 (Fig. 8D). High Ba/Th is widely observed in arc volcanic rocks, and is usually interpreted to reflect effects of aqueous fluids (Tatsumi et al., 1986), which mobilize Ba out of the subducting plate more efficiently than less soluble elements (e.g., Hawkesworth et al., 1993; Turner et al., 1996; Elliot et al., 1997; Tollstrup et al., 2010). An inverse relationship between Ba/Th and La/Sm, which has been documented in compilations of arc lava geochemistry (Turner et al., 2003; Labanieh et al., 2012), is well expressed in Mutnovsky–Gorely and other Kamchatka samples (Fig. 14). This and similar relationships have been widely interpreted to originate by mixing of subducted components with mantle peridotite. The subducted components are often interpreted to be hydrous fluids from subducted oceanic crust, and partial melts of subducted sediment (Hawkesworth et al., 1993; Turner et al., 1996, 2003; Elliot et al., 1997; Labanieh et al., 2012). Fig. 15 illustrates how these subducted components can be mixed with the mantle to explain the compositions of Kamchatka lavas in Ba/Th–La/Sm space. However, it is important to note that the Ba/Th–La/Sm plot does not reveal all of the source components that may be present in Kamchatka lavas. In particular, partial melts of subducted basalt under eclogite conditions, which are interpreted to be present in many Kamchatka lavas (Yogodzinski et al., 2001; Dosseto et al., 2003; Portnyagin et al., 2007a, 2007b; Bryant et al., 2011), are expected to have low Ba/Th and moderate La/Sm, and so fall approximately on a mixing lines between depleted mantle and partial melts of Kamchatka sediment (Fig. 17). This means that even if partial melts of subducting oceanic crust (MORB eclogite melts) are

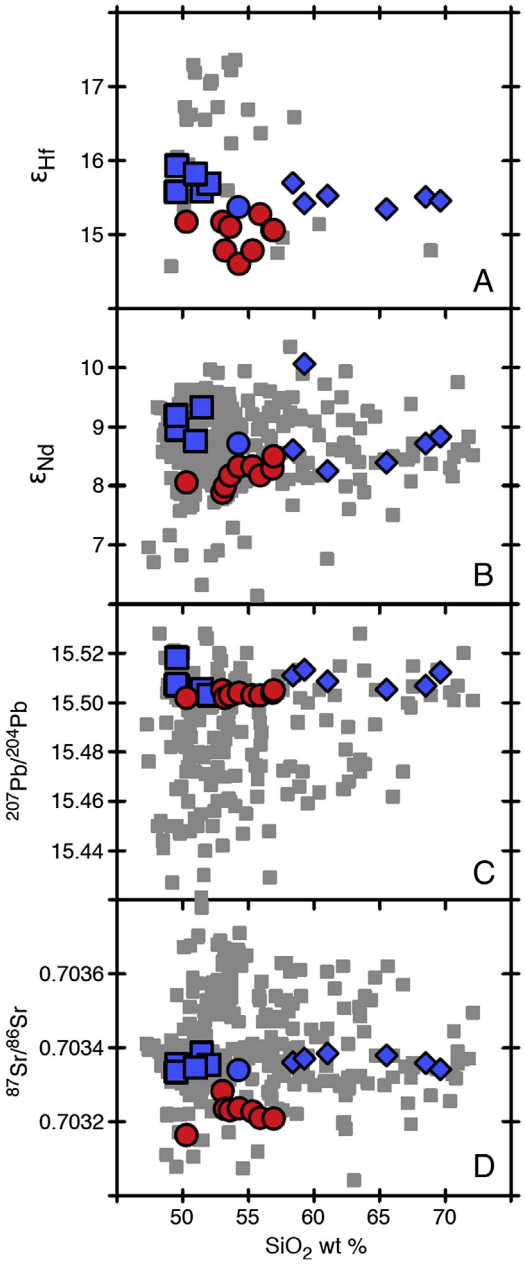

Fig. 12. Hafnium, Nd, Pb and Sr isotope ratios versus SiO_2 for Mutnovsky and Gorely samples. Other Kamchatka data are from sources cited in the caption of Fig. 3.

present in Kamchatka lavas, their effects will not be evident on this plot (Figs. 14–15).

Using trace element ratios only, the presence of a MORB eclogite melt component in Kamchatka lavas may be more evident in a plot of Th/La versus Yb/La, which separates the eclogite components (fluids and melts of subducting oceanic crust) from partial melts of the mantle and sediment (Fig. 18). On this plot, and in Figs. 16–17, we show the compositions of Mutnovsky and Gorely basalts and basaltic andesites only, because the more mafic compositions show similar variability in trace element ratios, which appear to have been unaffected by FC and AFC processes (Fig. 18). Because mixing lines in Fig. 18 are straight, and assuming that melting of the mantle wedge occurs primarily in the spinel field (i.e., mantle melting is garnet-absent), the data pattern in Fig. 18 may be interpreted to indicate that a significant portion of the Th and REEs present in Kamchatka lavas is derived from either fluids or melts of subducted oceanic crust.

This conclusion is well supported by data from Mutnovsky and Gorely and other Kamchatka lavas, which have highly variable trace element ratios, but uniformly radiogenic Nd and Hf isotopes (Fig. 19). For trace element ratios involving soluble elements, the extraction of aqueous fluids from subducted oceanic crust may explain the observed variation, because ratios such as Ba/Th are elevated in seawater-altered oceanic crust compared to fresh MORB (Kelley et al., 2003), whereas the Nd isotopic composition of seawater-altered oceanic crust is essentially the same as fresh MORB (Chauvel et al., 2009). Thus, fluid extraction from seawater-altered oceanic crust, can readily explain strong variation in Ba/Th in Kamchatka lavas that all have the similar and radiogenic Nd isotope compositions (Churikova et al., 2001).

It is less clear why we observe the same pattern in plots of Nd isotopes against ratios that pair two insoluble trace elements such as Hf/Nd (Fig. 19B). Unlike the case of Ba/Th, trace element ratios like Hf/Nd are similar in seawater-altered oceanic crust and fresh MORB (Kelley et al., 2003). This means that effects of seawater alteration of subducting oceanic crust cannot explain variability in Hf/Nd at nearly constant Nd isotope compositions. Mixing from MORB or depleted mantle toward subducted sediment or sediment melt compositions (Fig. 19B) also cannot explain variation in Hf/Nd at nearly constant ε_{Nd}. This is evident because mixing lines in Fig. 19B are straight, so it's clear that no binary mixture of MORB or depleted mantle with subducted sediment or sediment melt can pass through the compositions of Mutnovsky–Gorely and other Kamchatka lavas. Similar patterns are evident in plots of Hf isotopes against Nd/Hf and Ce/Hf (Fig. 19C–D). Fewer data points are available for the Hf isotope system, but again, mixing lines on these plots are straight, so it's evident that mixtures of MORB or depleted mantle and subducted sediment or sediment melt cannot explain the compositions of Kamchatka lavas. Based on this analysis we conclude that subduction-related trace element patterns in Kamchatka lavas are produced with minimal effect of subducted sediment, even though the presence of sediment is required by Pb isotope variation in Kamchatka lavas, which define a mixing line between subducted basalt and subducted sediment compositions in Pb–Pb isotope space (Fig. 11, see also Duggen et al., 2007).

Based on the previous discussion we conclude that a third source component, which is in addition to depleted mantle and subducted sediment, will also generally be required to explain the source mixture for Kamchatka lavas. This source component has both radiogenic Nd and Hf (similar to MORB) and fractionated Nd–Hf and Ce–Hf ratios (like arc lavas worldwide). Because elements such as Hf, Ce and Nd are relatively insoluble, their abundances in subduction-related, aqueous fluids are typically a factor of 10 or more below those in silicate melts (Tatsumi et al., 1986; Brenan et al., 1995; Kessel et al., 2005; Spandler et al., 2007). This has lead to the widespread conclusion that aqueous fluids do not transport significant quantities of Hf, Zr and light REEs out of the basaltic part of the subducting oceanic crust (Turner et al., 1996; Elliot et al., 1997; Pearce et al., 1999; Class et al., 2000). This leads us to conclude that fractionation of the insoluble trace element ratios in Kamchatka lavas compared to those in MORB (Hf/Nd, Ce/Hf, Fig. 19) are most likely to have resulted from extraction of hydrous partial melts from subducting oceanic crust. Observed fractionation of trace element ratios in Kamchatka could also be produced during extraction of solute-rich, supercritical liquids from subducting oceanic crust, because they have geochemical effects on trace element partitioning which are indistinguishable from those of silicate melts (Schmidt et al., 2004; Kessel et al., 2005).

These results are similar to those from recent studies in the Aleutian island arc (Yogodzinski et al., in press), the in rear-arc lavas of Isu–Bonin system (Tollstrup et al., 2010) and in the Central Kamchatka Depression (Portnyagin et al., 2007a, 2007b). In each of these cases, geochemical data have been used to show that the source mixture that produces arc magmas includes a significant contribution from partial melts of an isotopically depleted mantle wedge and from similarly depleted

Table 3
XLFRAC model results for fractional crystallization (FC) and assimilation-fractional crystallization (AFC). Two models are presented and each uses major and rare earth element (REE) compositions of Mutnovsky samples as indicated. Model 1 results indicate that 20% fractional crystallization (FC) of 6% olivine, 3% clinopyroxene and 91% plagioclase from basalt (CM-48), and assimilation (mixing) of a dacite (CM-47) component in a ratio of 9:1 (basalt:dacite) results in a composition that is similar to basaltic andesite sample M1-06-08. The sum of the squares of residuals is 1.63. The compositions of mineral phases were determined by using electron probe microanalysis with a 15 kV accelerating voltage, a 10 nA Faraday cup current and a beam diameter of 10 μm.

Model 1	Input						XLFRAC model		
	Clinopyroxene	Olivine	Plagioclase	CM-48 basalt	CM-47 dacite		Model rock	M1-06-08 observed	Difference
SiO_2	49.16	37.39	53.05	50.92	65.52	SiO_2	54.23	54.08	−0.15
TiO_2	0.92	0.00	0	1.31	0.92	TiO_2	1.34	1.34	0.00
Al_2O_3	3.42	0.11	30.01	17.46	16.25	Al_2O_3	17.66	17.61	−0.05
FeO	13.39	22.04	0.1	11.83	5.41	FeO	10.83	10.80	−0.03
MnO	0.43	0.34	0	0.24	0.15	MnO	0.23	0.23	0.00
MgO	14.32	39.47	0	4.89	1.64	MgO	3.51	3.50	−0.01
CaO	18.00	0.28	12.38	9.54	4.07	CaO	8.29	8.22	−0.07
Na_2O	37.00	0.02	4.56	3.12	3.81	Na_2O	3.51	3.50	−0.01
K_2O	0.00	0.34	0	0.36	2.01	K_2O	0.45	0.45	0.00
						La	6.48	6.46	−0.02
						Ce	17.80	17.80	0.00
						Nd	16.40	16.40	0.00
						Sm	5.13	5.12	−0.01
						Eu	1.90	1.89	−0.01
						Gd	6.74	6.72	−0.02
						Dy	7.88	7.86	−0.02
						Er	4.81	4.80	−0.01
						Yb	4.72	4.71	−0.01

Model 2	Input			M1-06-08	CM-47		CM-24	XLFRAC model	
	Clinopyroxene	Orthopyroxne	Plagioclase	Basaltic andesite	Dacite CM-47		Model rock	CM-24 observed	Difference
SiO_2	50.669	51.974	53.05	54.08	65.52	SiO_2	61.11	60.73	−0.38
TiO_2	0.722	0.285	0	1.34	0.92	TiO_2	0.52	1.03	0.51
Al_2O_3	2.591	0.55	30.01	17.61	16.25	Al_2O_3	18.26	18.28	0.02
FeO	17.185	23.346	0.1	10.80	5.41	FeO	6.42	6.20	−0.22
MnO	0.624	0.856	0	0.23	0.15	MnO	0.16	0.16	0.00
MgO	15.959	20.282	0	3.50	1.64	MgO	2.01	2.23	0.22
CaO	13.227	3.415	12.38	8.22	4.07	CaO	6.23	5.59	−0.64
Na_2O	0.216	0.1	4.56	3.50	3.81	Na_2O	3.82	4.42	0.60
K_2O	0	0.017	0	0.45	2.01	K_2O	1.34	1.04	−0.30
						La	10.10	8.21	−1.89
						Ce	26.10	23.90	−2.20
						Nd	19.00	19.30	0.30
						Sm	5.15	5.62	0.47
						Eu	1.50	1.83	0.33
						Gd	6.03	6.59	0.56
						Dy	6.56	7.36	0.80
						Er	3.90	4.42	0.52
						Yb	3.90	4.59	0.69

Model 2 results indicate that 11% FC of 100% plagioclase from basaltic andesite M1-06-08, and assimilation (mixing) of a dacite (CM-47) component in a ratio of 6:4 (basaltic andesite: dacite) produces an andesite composition that is similar to andesite sample CM-24. The sum of the squares of residuals is 0.887.

subducting oceanic crust. Portnyagin et al. (2007a, 2007b) and Yogodzinski et al. (in press) refer to this as an eclogite melt source component, and we adopt this terminology for the remainder of this discussion.

Duggen et al. (2007) and Tollstrup et al. (2010) showed that lavas from arc-front volcanoes carry the geochemical signature of hydrous fluids from subducting oceanic crust (e.g., high Ba/Th), and argued that only lavas from the rear-arc volcanoes show the effects of the eclogite melt component. This conclusion is based on the presence of strong enrichments of fluid-soluble elements in volcanic-front lavas, which are diminished in lavas from rear-arc volcanoes. Our data confirm this pattern for Mutnovsky compared to Gorely, which are well separated on the Ba/Th versus La/Sm plot (Fig. 16). This pattern, and in particular the high Ba/Th seen in Mutnovsky lavas, cannot be explained by alteration of subducting oceanic crust, which produces only a modest increase Ba/Th compared to trace element ratios such as Ce/Th, U/Th

Table 4
Partition coefficients used for geochemical modeling described in this study, in addition to those referenced in the text.

Element	Plagioclase	Clinopyroxene	Olivine	Orthopyroxene	Hornblende	Garnet	Ilmenite	Magnetite
La	0.2	0.1	0.001	0.003	0.17	0.01	0.001	0.003
Ce	0.18	0.15	0.001	0.006	0.44	0.02	0.001	0.003
Nd	0.14	0.2	0.001	0.01	0.76	0.09	0.001	0.003
Sm	0.11	0.25	0.001	0.012	1.2	0.22	0.001	0.003
Eu	0.1	0.27	0.001	0.015	1.4	0.33	0.001	0.003
Gd	0.09	0.29	0.001	0.017	1.7	0.5	0.001	0.003
Dy	0.07	0.31	0.001	0.025	2.1	1.06	0.001	0.003
Er	0.05	0.33	0.001	0.035	2	2.15	0.001	0.003
Yb	0.03	0.35	0.001	0.05	2	4	0.001	0.003
Y	0.05	0.33	0.001	0.025	2.1	1.06	0.001	0.003

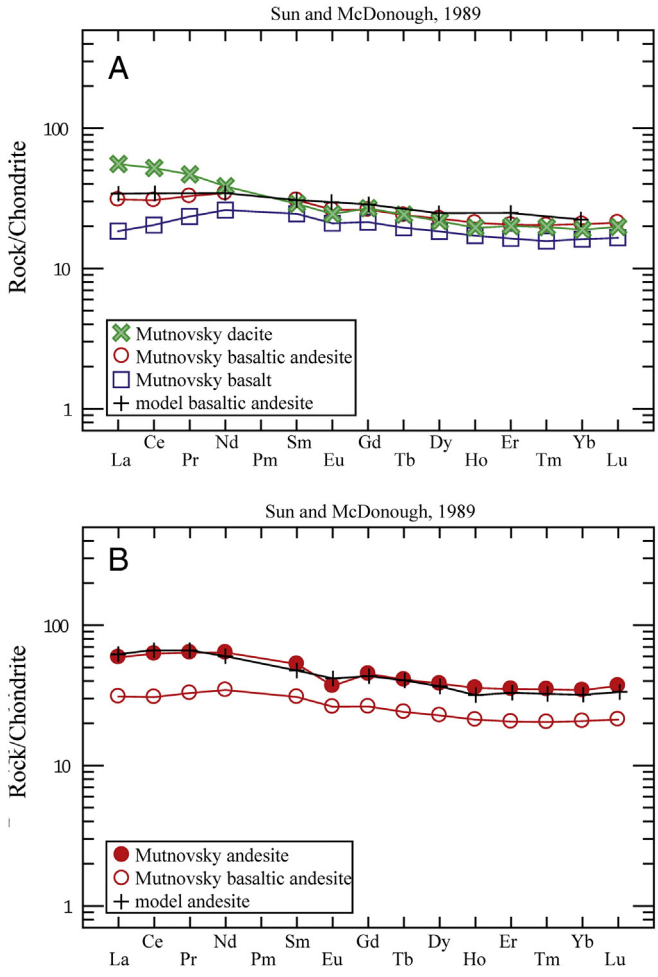

Fig. 13. Model AFC results, generated using the rare earth element (REE) abundances of Mutnovsky volcanic rocks as indicated in Table 3. In panel A, model basaltic andesite (crosses) produced by 20% fractional crystallization (FC) of 6% olivine, 3% clinopyroxene and 91% plagioclase from basalt CM-48 (boxes), and assimilation (mixing) of a dacite CM-47 (x's) component in a ratio of 9:1 (basalt:dacite) results in a composition that is similar to basaltic andesite sample M1-06-08 (circles); the composition of Mutnovsky basaltic andesite CM-105 is shown as red open circles. In panel B, model andesite (black crosses) produced by 11% FC of 100% plagioclase from basaltic andesite M1-06-08 (open circles), and assimilation (mixing) of a dacite CM-47 (x's) component in a ratio of 6:4 (basaltic andesite:dacite) produces an andesite composition that is similar to andesite sample CM-24. Details of AFC calculations are provided in the text and Table 3. (For interpretation of the references to color in this figure legend, the reader is referred to the web version of this article.)

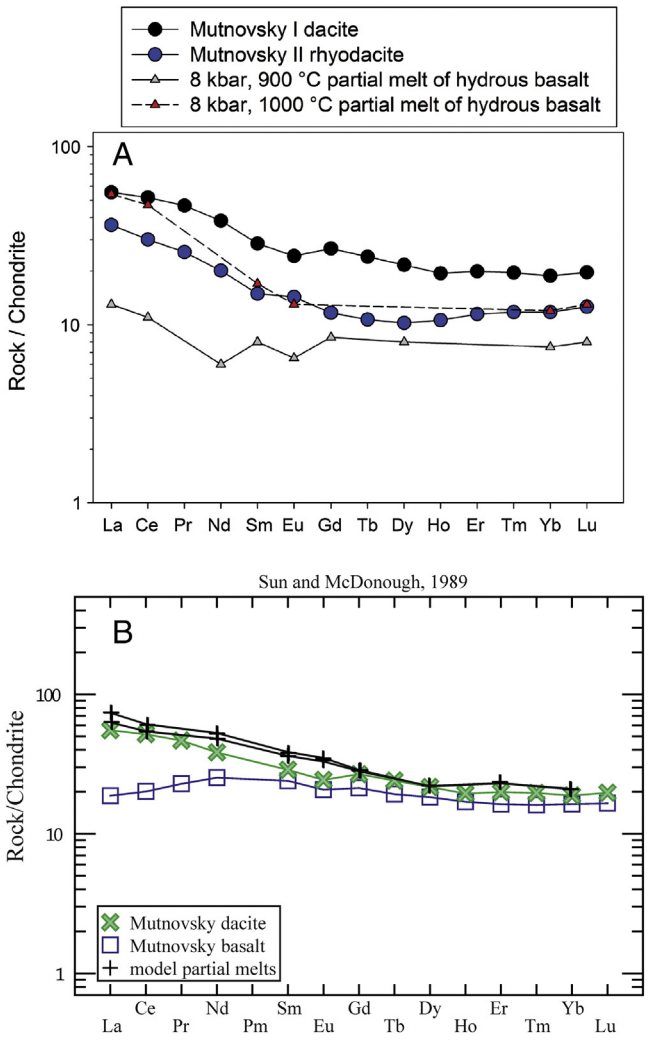

Fig. 14. A) The REE chemistry of dacites (CM-47) and (CM-113) from Mutnovsky I, and II, respectively, compared with REE chemistry of partial melts produced by vapor-absent partial melting experiments (Rapp et al., 1991) of amphibole-bearing basaltic rock at 8 kbar, 900 °C and 8 kbar, 1000 °C. B) Model results for the evolution of REE abundances of silicate melt produced by batch melting hornblende-bearing basaltic rock (squares) with a composition of basalt M1-04-08 to produce dacite CM-47 (x's). Two model results are shown with + symbols: Model 1 (upper + 's) is for 20% batch melting of a basaltic rock that contains 60% clinopyroxene, 10% olivine, and 30% hornblende. Model 2 (lower + 's) is for 25% batch melting of the same basaltic rock.

and Rb/Th, which are dramatically increased in seawater-altered oceanic crust compared to fresh MORB (e.g., Fig. 5 in Kelley et al., 2003). This means that high Ba/Th values greater than ~100 in island arc magmas must be linked to a hydrous fluid source component that is likely extracted from subducted basalt at temperatures below the water-saturated solidus (Hawkesworth et al., 1993; Turner et al., 1996; Elliot et al., 1997). These characteristics for such a fluid are consistent with recent eclogite melting experiments (Kessel et al., 2005) as shown in our MORB eclogite fluid model (Fig. 17). We conclude that the eclogite source component (which again, is produced by partial melting of subducted basalt in the eclogite facies) contributes to both arc-front and rear-arc magmas because the Hf–Nd isotope plots against insoluble trace element ratios show nearly identical patterns for Mutnovsky and Gorely samples (Fig. 19B–D). These patterns clearly require a third source component that has radiogenic Nd and Hf (similar to MORB) but also fractionated Nd–Hf and Ce–Hf abundance ratios (like those of arc volcanic rocks).

If this interpretation is correct it probably means the hydrous fluid component diminishes from the arc front to rear arc, as the subducting plate sinks and is heated and as the eclogite melt component grows. This change from Mutnovsky to Goreley is broadly consistent with arc-front to rear-arc changes observed throughout the Isu–Bonin and Tonga–Kermadec arc systems (Tollstrup et al., 2010; Todd et al., 2010). Based on these spatial–geochemical patterns we speculate that the water in these two source components may enter the subduction zones by separate pathways. Specifically, it seems likely that intensely serpentinized peridotite, which forms beneath the forearc and above the subducting plate, is probably often carried into the area of melt formation below the volcanic front (Savov et al., 2005; Savov et al., 2007). This mixed serpentinite material, which is present at the surface in forearc serpentinite volcanoes (Savov et al., 2005; Savov et al., 2007), may be the source of high Ba/Th aqueous fluids that are prominent in the arc front at Mutnovsky, and along the arc front throughout the Isu–Bonin and Tonga–Kermadec systems, but which diminish in

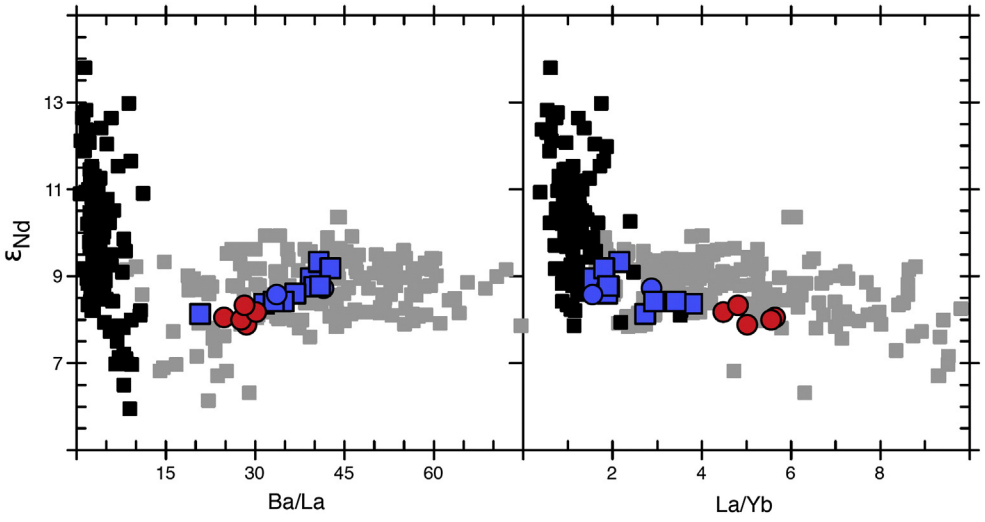

Fig. 15. Plot of Nd isotopes against Ba/La and La/Yb for Mutnovsky and Gorely basalts and basaltic andesites compared with other Kamchatka lavas. Symbols and data sources here are the same as in Fig. 9.

importance from the arc front to the backarc (Duggen et al., 2007; Tollstrup et al., 2010; Todd et al., 2010). In contrast, the water that must also be present in the eclogite melt component may be derived from serpentinized peridotite formed within the subducting plate. This serpentinite is created by bending-related faults on the outer rise and on the outer trench wall, as the subducting plate enters the trench (Ranero et al., 2003; Ranero and Sallarés, 2004). Serpentinites formed by this process appear to penetrate to depths of greater than 20 km below the surface of the subducting oceanic lithosphere. Dewatering of serpentinites in the mantle section of the subducting plate, could then induce melting within the overlying crust, and by this process, create the eclogite melt component.

6. Conclusions

1) Least-squares assimilation-fractional crystallization models for major elements and REE are consistent with Mutnovsky basaltic andesites originating by fractional crystallization of plagioclase, clinopyroxene and olivine combined with assimilation of dacite. Model results indicate that andesites are plausibly produced by fractional crystallization of plagioclase from basaltic andesite, combined with assimilation of dacite.

2) Mutnovsky dacites have nearly identical Sr, Nd and Pb isotope signatures as more mafic lavas. A plausible origin for the dacites involves partial melting of previously emplaced (underplated) amphibole-bearing basaltic magma at mid-crustal PT conditions. This is

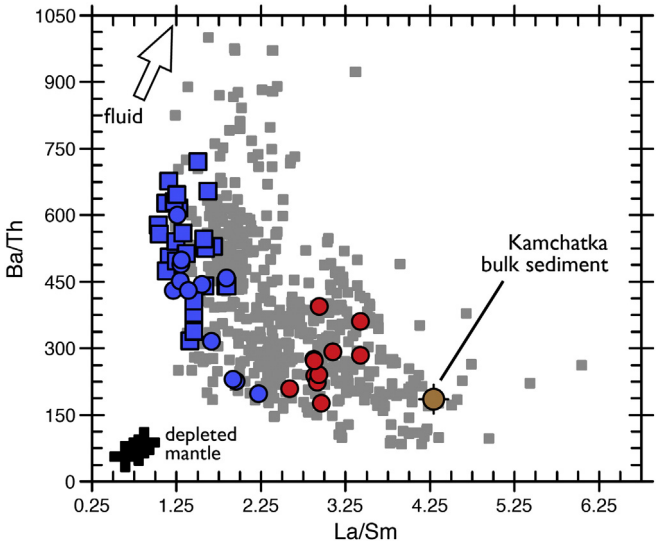

Fig. 16. Plot of Ba/Th versus La/Yb comparing basalts and basaltic andesites from Mutnovsky, Gorely with other Kamchatka lavas and with depleted mantle and Kamchatka sediment. Depleted mantle compositions are from Salters and Stracke (2003) and Workman and Hart (2005). Kamchatka sediment is from Plank & Langmuir (1998). Other symbols are the same as in Fig. 9. This figure is modified from Labanieh et al. (2012).

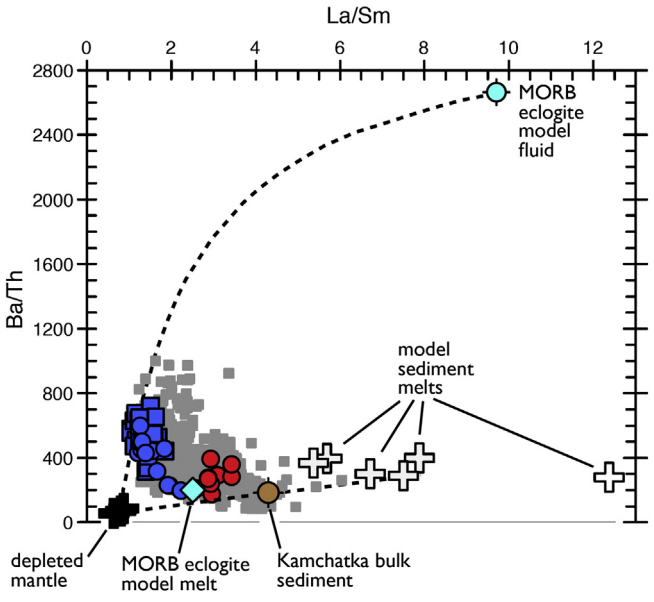

Fig. 17. Plot of Ba/Th versus La/Sm comparing Mutnovsky, Gorely and other Kamchatka lavas with depleted mantle, Kamchatka sediment and model compositions for sediment melts, MORB eclogite melts and MORB eclogite fluids. Model eclogite fluid is derived from average MORB using partitioning data from Kessel et al. (2007) experiments at 4 GPa and 700 °C. Model eclogite melt is derived from average MORB with partitioning from Kessel et al. (2005) experiments at 4 GPa and 900 °C. Model sediment melts are derived from Kamchatka bulk sediment from Plank and Langmuir (1998), using melt/bulk sediment enrichment factors from sediment melting experiments of Skora and Blundy (2010) and Hermann and Rubatto (2009) conducted at 800–900 °C and 2.5–3.5 GPa. Dashed lines show mixing trajectories from depleted mantle to MORB eclogite fluid and to average sediment melt compositions. Sources of other data are the same as in Fig. 3.

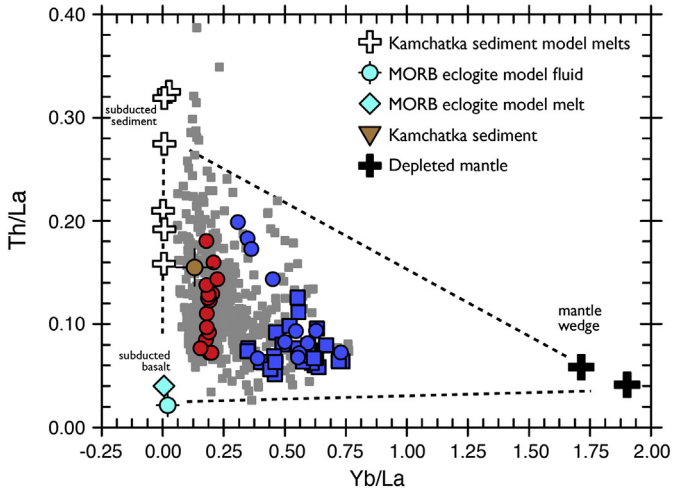

Fig. 18. Plot of Th/La versus Yb/La comparing basalts and basaltic andesites from Mutnovsky and Gorely with other Kamchatka lavas and with depleted mantle, Kamchatka sediment and model compositions for sediment melts, MORB eclogite melts and MORB eclogite fluids. Dashed lines show mixing paths between source components in subducted sediment, depleted mantle, and subducted basalt. Model compositions for eclogite fluid, eclogite melt and sediment melt are the same as in Fig. 15. Other symbols and data sources are the same as in Fig. 3.

consistent with the isotope signature of the dacites and also model batch melting results and published experimental partial melt data.

3) Strong fractionation among insoluble trace elements (e.g., Nd/Hf, Ce/Hf) in Mutnovsky, Gorely and most other Kamchatka lavas is produced at nearly constant and highly radiogenic Nd and Hf isotopic compositions, with virtually no influence from subducted sediment. Assuming that aqueous fluids from the subducting oceanic crust cannot carry significant quantities of these relatively insoluble elements, the observed patterns require that partial melting of subducting oceanic crust is occurring beneath Kamchatka, and that the resulting hydrous melts of MORB eclogite exert primary control over the abundances of key trace elements such as Hf, Zr and light REEs in Kamchatka lavas.

Acknowledgments

ACS acknowledges support from NSF grants EAR 1264537 and 1264560. This work was also supported by NSF grants EAR 0236481, EAR 0310146 and OCE 0728077 to GMY. ES acknowledges support from NSF grant EAR 1016100. Helpful reviews by Maxim Portnyagin and Mariek Schmidt greatly improved the quality of this paper. Thanks also to Mac Rutherford for his efficient editorial handling of the paper, and also to Ivan Savov, for his thoughtful input. We thank Ilya Bindeman for analyzing olivines for $\delta^{18}O$ and Racheal Johnsen for her help with

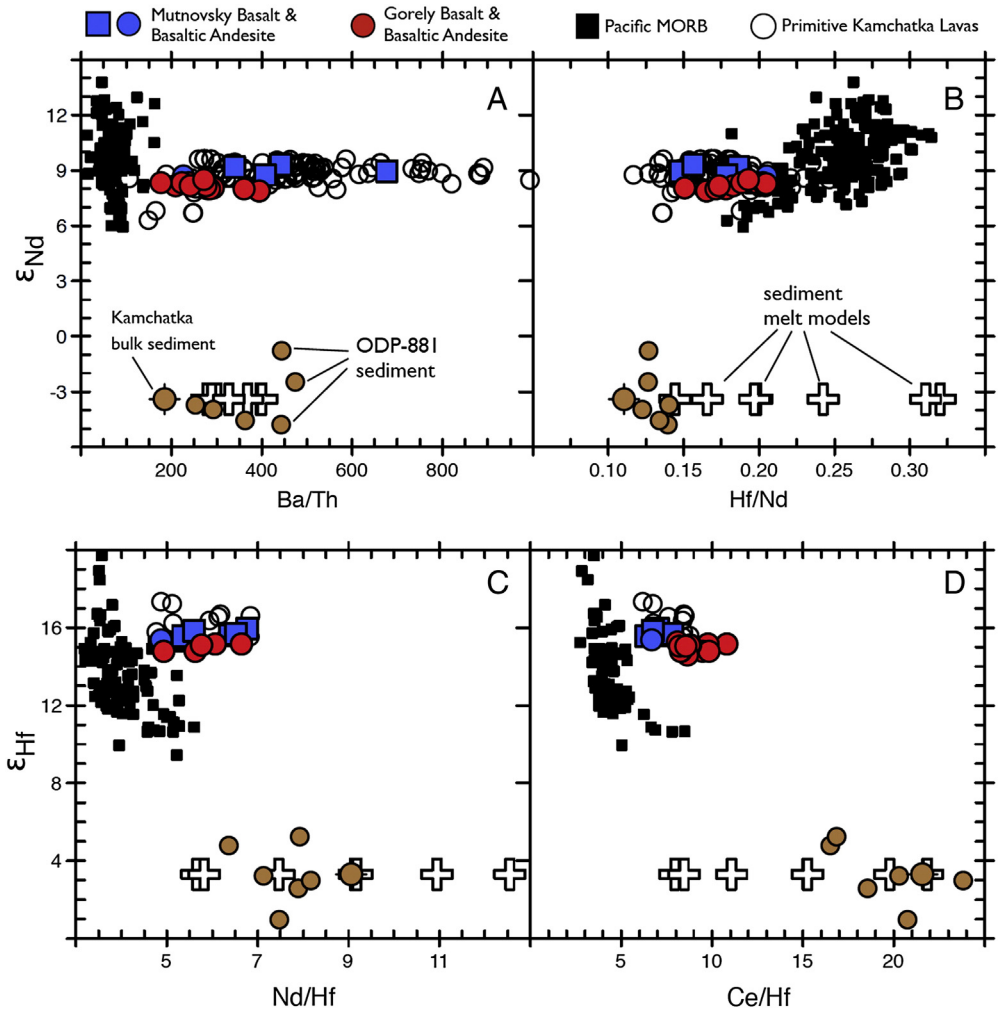

Fig. 19. Plot of Nd isotopes (ε_{Nd}) against trace element ratios Ba/Th and Hf/Nd, and Hf isotopes (ε_{Hf}) against trace element ratios Nd/Hf and Ce/Hf. Primitive MORB compositions are samples with >8% MgO and $^{87}Sr/^{86}Sr$ <0.7030 from PetDB expert compilation by Class and Lehnert (2012). Other symbols and data sources are the same as in Fig. 3.

whole-rock isotope analyses at the University of Kansas. The assistance of Max Siegrist and Beth Bair for their help with trace element and Hf isotope data acquisition at the University of South Carolina is also gratefully acknowledged. Tatiana Rychkova, Anatoly Mushinsky, and Denise Honn all provided valuable assistance in the field. This work was supported by a University of Nevada Las Vegas President's Research Award, and the University of Nevada Las Vegas President's Graduate Fellowship, the Nevada Stars Graduate Fellowship, and ExxonMobil Scholarship to KLR.

Appendix A. Supplementary data

Supplementary data to this article can be found online at http://dx.doi.org/10.1016/j.jvolgeores.2014.09.003.

References

Abratis, M., Wörner, G., 2001. Ridge collision, slab-window formation, and the flux of Pacific asthenosphere into the Caribbean realm. Geology 29, 127–130.
Almeev, R.R., Kimura, J.I., Ariskin, A.A., Ozerov, A.Y., 2013. Decoding crystal fractionation in calc-alkaline magmas from the Bezymianny Volcano (Kamchatka, Russia) using mineral and bulk rock compositions. J. Volcanol. Geotherm. Res. 263, 141–171.
Alves, S., Schiano, P., Allégre, C., 1999. Rhenium–osmiium isotopic investigation of Java subduction zone lavas. Earth Planet. Sci. Lett. 168, 65–77.
Atherton, M.P., Petford, N., 1993. Generation of sodium-rich magmas from newly underplated basaltic crust. Nature 362, 144–146.
Avdeiko, G.P., Savelyev, D.P., Palueva, A.A., Popruzhenko, S.V., 2007. Evolution of the Kurile–Kamchatkan volcanic arcs and dynamics of the Kamchatkan–Aleutian junction. Geophys. Monogr. Ser. 172, 37–55.
Bach, W., Hegner, E., Erzinger, J., Satir, M., 1994. Chemical and isotopic variations along the superfast spreading East Pacific Rise from 6 to 30°S. Contrib. Mineral. Petrol. 116, 365–380.
Beard, J.S., Lofgren, G.E., 1989. Effect of water on the composition of partial melts of greenstone and amphibolite. Science 244, 195–197.
Beard, J.S., Lofgren, G.E., 1991. Dehydration melting and water-saturated melting of basaltic and andesitic greenstones and amphibolites at 1, 3 and 6.9 kb. J. Petrol. 32 (2), 365–401.
Bindeman, I., 2008. Oxygen isotopes in mantle and crustal magmas as revealed by single crystal analysis. In: Putirka, K.D., Tepley, F.J. (Eds.), Reviews in Mineralogy and Geochemistry 69, pp. 445–478.
Bindeman, I.N., Bailey, J.C., 1999. Trace elements in anorthite megacrysts from the Kurile Island Arc: a window to across-arc geochemical variations in magma compositions. Earth Planet. Sci. Lett. 169, 209–226.
Bindeman, I.N., Ponomareva, V.V., Bailey, J.C., Valley, J.W., 2004. Volcanic arc of Kamchatka: a province with high-$\delta^{18}O$ magma sources and large-scale $^{18}O/^{16}O$ depletion of the upper crust. Geochim. Cosmochim. Acta 68, 841–865.
Bindeman, I.N., Eiler, J.M., Yogodzinski, G.M., Tatsumi, Y., Stern, C.R., Grove, T.L., Portnyagin, M., Hoernle, K., Danyushevsky, L.V., 2005. Oxygen isotope evidence for slab melting in modern and ancient subduction zones. Earth Planet. Sci. Lett. 235, 480–496.
Bindeman, I.N., Leonov, V.I., Izbekov, P.E., Ponomareva, V.V., Watts, K.E., Shipley, N.K., Perepelov, A.B., Bazanova, L.I., Jicha, B.R., Inger, B.S., Schmitt, A.K., Portnyagin, M.V., Chen, C.H., 2010. Large-volume silicic volcanism in Kamchatka: Ar–Ar and U–Pb ages, isotopic, and geochemical characteristics of major pre-Holocene caldera-forming eruptions. J. Volcanol. Geotherm. Res. 189, 57–80.
Borg, L.E., Clynne, M.A., 1998. The petrogenesis of felsic calc-alkaline magmas from the southernmost Cascades, California: origin by partial melting of basaltic lower crust. J. Petrol. 39 (6), 1197–1222.
Bourdon, E., Eissen, J.-P., Monzier, M., Robin, C., Martin, H., Cotton, J., Hall, M.L., 2002. Adakite-like lavas from Antisana Volcano (Ecuador): evidence for slab melt metosomatism beneath Andean northern volcanic zone. J. Petrol. 43 (2), 199–217.
Bouvier, A.-S., Metrich, N., Deloule, E., 2008. Slab-derived fluids in the magma sources of St. Vincent (Lesser Antilles Arc): volatile and light element imprints. J. Petrol. 49 (8), 1427–1448.
Braitseva, O.A., Melekestsev, I.V., Ponomareva, V.V., 1992. Tephra of the largest prehistoric holocene volcanic eruptions in Kamchatka. Quat. Int. 13 (14), 177–180.
Braitseva, O.A., Melekestsev, I.V., Ponomareva, V.V., Kirianov, V.Yu., 1996. The caldera-forming eruption of Ksudach volcano about ca. AD 240, the greatest explosive event of our era in Kamchatka. J. Volcanol. Geotherm. Res. 70, 49–66.
Brenan, J.M., Shaw, H.F., Ryerson, F.J., Phinney, D.L., 1995. Mineral-aqueous fluid partitioning of trace elements at 900 °C and 2.0 GPa: constraints on the trace element chemistry of mantle and deep crustal fluids. Geochim. Cosmochim. Acta 59, 3331–3350.
Bryant, J.A., Yogodzinski, G.M., Churikova, T., 2007. Evidence of melt–mantle interaction from ultramafic xenoliths from Shiveluch Volcano, Kamchatka. Geochem. Geophys. Geosyst. http://dx.doi.org/10.1029/2006GC001443 (p. 24 pages).
Bryant, J.A., Yogodzinski, G.M., Churikova, T.G., 2011. High-Mg# andesitic lavas of the Shisheisky Complex, Northern Kamchatka: implications for primitive calc-alkaline magmatism. Contrib. Mineral. Petrol. 161, 791–810.
Carr, M., 2007. Igpet 2007 for Windows XP or Vista. Terra Softa Inc.
Castillo, P.R., Natland, J.H., Niu, Y., Lonsdale, P.F., 1998. Sr, Nd, and Pb isotopic variation along the Pacific-Antarctic risecrest, 53°–57°S: implications for the composition and dynamics of the South Pacific upper mantle. Earth Planet. Sci. Lett. 154, 109–125.
Castillo, P.R., Klein, E., Bender, J., Langmuir, C., Shirey, S., Batiza, R., White, W., 2000. Petrology and Sr, Nd, and Pb isotope geochemistry of mid-ocean ridge basalt glasses from the 11,45°N to 15,00°N segment of the East Pacific Rise. Geochem. Geophys. Geosyst. 1. http://dx.doi.org/10.1029/1999GC000024.
Chauvel, C., Blichert-Toft, J., 2001. A hafnium isotope and trace element perspective on melting of the depleted mantle. Earth Planet. Sci. Lett. 190, 137–151.
Chauvel, C., Marini, J.C., Plank, T., Ludden, J.N., 2009. Hf–Nd input flux in the Izu–Mariana subduction zone and recycling of subducted material in the mantle. Geochem. Geophys. Geosyst. 10. http://dx.doi.org/10.1029/2008GC002101.
Cheatham, M.M., Sangrey, W.F., White, W.M., 1993. Sources of error in external calibration ICP-MS analysis of geological samples and an improved non-linear drift correction procedure: Spectrochimica Acta, v. v 48bpp, E487–E506.
Churikova, T., Dorendorf, F., Wörner, G., 2001. Sources and fluids in the mantle wedge below Kamchatka, evidence from across-arc geochemical variation. J. Petrol. 42, 1567–1593.
Churikova, T., Gordeichik, B.N., Ivanov, B.V., 2012. Petrochemistry of Kamen Volcano: a comparison with neighboring volcanoes of the Klyuchevskoy Group. J. Volcanol. Seismol. 6, 150–171.
Class, C., Lehnert, K., 2012. PetDB Expert MORB (Mid-Ocean Ridge Basalt) Compilation. http://dx.doi.org/10.1594/IEDA/100060.
Class, C., Miller, D.M., Goldstein, S.L., Langmuir, C.H., 2000. Distinguishing melt and fluid subduction components in Umnak Volcanics. Aleutian ArcGeochemistry, Geophysics, Geosystems (paper number 1999GC000010).
Coleman, D.S., Frost, T.P., Glazner, A.F., 1992. Evidence from the Lamarck Granodiorite for rapid Late Cretaceous crust formation in California. Science 258, 1924–1926.
Conrad, W.K., Kay, R.W., 1984. Ultramafic and mafic inclusions from Adak Island: crystallization history, and implications for the nature of primary magmas and crustal evolution in the Aleutian arc. J. Petrol. 25, 88–125.
Davidson, J.P., Turner, S., Handley, H., Macpherson, C., Dosseto, A., 2007. Amphibole "sponge" in arc crust? Geology 35, 787–790.
Davis, A.S., Clague, D.A., Cousens, B.L., Keaten, R., Paduan, J.B., 2008. Geochemistry of basalt from the North Gorda segment of the Gorda Ridge: evolution toward ultraslow spreading ridge lavas due to decreasing magma supply. Geochem. Geophys. Geosyst. http://dx.doi.org/10.1029/2007GC001775.
Dickinson, W.R., Hatherton, T., 1967. Andesitic volcanism and seismicity around the Pacific. Science 74, 801–803.
Dirksen, O., Humphreys, M.C.S., Pletchov, P., Melnik, O., Demyanchuk, Y., Sparks, R.S.J., Mahony, S., 2006. The 2001–2004 dome-forming eruption of Shiveluch Volcano, Kamchatka: observation, petrological investigation and numerical modelling. Journal of Volcanology and Geothermal Research 155 (3–4), 201–226.
Dorendorf, F., Wiechert, U., Woerner, G., 2000a. Hydrated sub-arc mantle: a source for the Klyuchevskoy volcano, Kamchatka/Russia. Earth Planet. Sci. Lett. 175, 69–86.
Dorendorf, F., Churikova, T., Koloskov, A., G., W., 2000b. Late Pleistocene to Holocene activity at Bakening volcano and surrounding monogenetic centers Kamchatka: volcanic geology and geochemical evolution. J. Volcanol. Geotherm. Res. 104, 131–151.
Dosseto, A., Bourdon, B., Joron, J.-L., Dupre', B., 2003. U–Th–Pa–Ra study of the Kamchatka arc: new constraints on the genesis of arc lavas. Geochim. Cosmochim. Acta 67 (15), 2857–2877.
Duggen, S., Portnyagin, M., Baker, J., Ulfbeck, D., Hoernle, K., Garbe-Schonberg, D., Grassineau, N., 2007. Drastic shift in lava geochemistry in the volcanic-front to rear-arc region of the Southern Kamchatkan subduction zone: evidence for the transition from slab surface dehydration to sediment melting. Geochim. Cosmochim. Acta 71, 452–480.
Elliot, T., Plank, T., Zindler, A., White, W., Bourdon, B., 1997. Element transport from slab to volcanic front at the Mariana Arc. J. Geophys. Res. 102, 14991–15019.
Fedotov, S.A., Markhinin, Y.K., 1983. The Great Tolbachik Fissure Eruption; Geological and Geophysical data 1975–1976: Cambridge. Cambridge Univerity Press, United Kingdom.
Fedotov, S.A., Masurenkov, Y.P., 1991. Active Volcanoes of Kamchatka. Nauka Publishers, Moscow (720 pp.).
Ferlito, C., 2011. Bimodal geochemical evolution at Shiveluch stratovolcano, Kamchatka, Russia: consequence of a complex subduction at the junction of the Kurile–Kamchatka and Aleutian island arcs. Earth-Sci. Rev. 105, 49–69.
Gill, J.B., 1981. Orogenic Andesites and Plate Tectonics. Springer-Verlag, Berlin, Heidelberg, New York (390 pp.).
Gorbach, N.V., Portnyagin, M.V., 2011a. Geology and petrology of the lava complex of Young Shiveluch Volcano, Kamchatka. Petrology 19, 134–166.
Gorbach, N.V., Portnyagin, M.V., 2011b. Geology and petrology of the lava complex of Young Shiveluch Volcano, Kamchatka. Petrology 19 (2), 134–166.
Gorbatov, A.G., 1997. Seismicity and structure of the Kamchatka subduction zone. J. Geophys. Res. Solid Earth 102 (B8), 17883–17898.
Gorbatov, A., Domínguez, J., Suárez, G., Kostoglodov, V., Zhao, D., Gordeev, E., 1999. Tomographic imaging of the P-wave velocity structure beneath the Kamchatka peninsula. Geophys. J. Int. 137, 269–279.
Goring, M.L., Kay, S.M., 2001. Mantle processes and sources of neogene slab window magmas from Southern Patagonia, Argentina. J. Petrol. 42 (6), 1067–1094.
Graham, D.W., Blichert-Toft, J., Russo, C.J., Rubin, K.H., Albarède, F., 2006. Cryptic striations in the upper mantle revealed by hafnium isotopes in southeast Indian ridge basalts. Nature 440, 199–202.
Grib, E.N., Leonov, V.L., Perepelov, A.B., 2009. The Karymskii Volcanic Center: volcanic rock geochemistry. J. Volcanol. Seismol. 3, 367–387.

Grove, T.L., Baker, M.B., Price, R.C., Parman, S.W., Elkins-Tanton, L.T., Chatterjee, N., Muntener, Othamar, 2005. Magnesian andesite and dacite lavas from Mt. Shasta, California: products of fractional crystallization of H_2O-rich mantle melts. Contrib. Mineral. Petrol. 148, 542–565.
Hahm, D., Castillo, P.R., Hilton, D.R., 2009. A deep mantle source for high 3He/4He ocean island basalts (OIB) inferred from Pacific near-ridge seamount lavas. Geophys. Res. Lett. 36. http://dx.doi.org/10.1029/2009GL040560.
Hamelin, C., Dosso, L., Hanan, B., Barrat, J.-A., Ondréas, H., 2010. Sr–Nd–Hf isotopes along the Pacific Antarctic Ridge from 41 to 53°S. Geophys. Res. Lett. http://dx.doi.org/10.1029/2010GL042979.
Hamelin, C., Doss, L., Hanan, B.B., Moreira, M., Kositsky, A.P., Thomas, M.Y., 2011. Geochemical portray of the Pacific Ridge: new isotopic data and statistical techniques. Earth Planet. Sci. Lett. 302, 154–162.
Hanan, B.B., Blichert-Toft, J., Pyle, D.G., Christie, D.M., 2004. Contrasting origins of the upper mantle revealed by hafnium and lead isotopes from the Southeast Indian Ridge. Nature 432, 91–94.
Hawkesworth, C.J., Gallagher, K., Hergt, J.M., McDermott, F., 1993. Mantle and slab contributions in arc magmas. Annu. Rev. Earth Planet. Sci. 21, 175–204.
Hegner, E., Tatsumoto, M., 1987. Pb, Sr, and Nd isotopes in basalts and sulfides from the Juan de Fuca Ridge. J. Geophys. Res. 92, 11380–11386.
Hermann, J., Rubatto, D., 2009. Accessory phase control on the trace element signature of sediment melts in subduction zones. Chem. Geol. 265, 512–526.
Hidalgo, P.J., Rooney, T.O., 2010. Crystal fractionation processes at Baru Volcano from the Deep to Shallow Crust. Geochem. Geophys. Geosyst. 11. http://dx.doi.org/10.1029/2010GC003262.
Hochstaedter, A.G., Kepezhinskas, P., Defant, M., Drummond, M., Koloskov, A., 1996. Insights into the volcanic arc mantle wedge from magnesian lavas from the Kamchatka arc. J. Geophys. Res. 101, 697–712.
Ishikawa, T., Tera, F., 1997. Source, composition and distribution of the fluid in the Kurile mantle wedge: constraints from across-arc variations of B/Nb and B isotopes. Earth Planet. Sci. Lett. 152, 123–138.
Ishikawa, T., Tera, F., Nakazawa, T., 2001. Boron isotope and trace element systematics of the three volcanic zones in the Kamchatka arc. Geochim. Cosmochim. Acta 65, 4523–4537.
Ishimaru, S., Arai, S., Y., I., Shirasaka, M., Okrugin, V.M., 2007. Melting and multi-stage metasomatism in the mantle wedge beneath a frontal arc inferred from highly depleted peridotite xenoliths from the Avacha Volcano southern Kamchatka. J. Petrol. 48. http://dx.doi.org/10.1093/petrology/egl065.
Ito, E., White, W.M., Göpel, C., 1987. The O, Sr Nd, and Pb isotope geochemistry of MORB. Chem. Geol. 62, 1957–1976.
Ivanov, A.V., Palesskii, S.V., Demonterova, E.I., Nikolaeva, I.V., Ashchepkov, I.V., Rasskazov, S.V., 2008. First data on the distribution of platinum-group elements (Ir, Os, Ru, Pt, and Pd) and Re in island-arc basalts of Kamchatka. Dokl. Earth Sci. 420, 597–601.
Izbekov, P.E., Eichelberger, J.C., Ivanov, B.V., 2004. The 1996 eruption of Karymsky Volcano, Kamchatka: historical record of basaltic replenishment of an andesite reservoir. J. Petrol. 45, 2325–2345.
Jakes, P., Gill, J., 1970. Rare earth elements and the island arc tholeiitic series. Earth Planet. Sci. Lett. 9, 17–28.
Janney, P.E., Le Roex, A.P., Carlson, R.W., 2005. Hafnium isotope and trace element constraints on the nature of mantle heterogeneity beneath the Central Southwest Indian Ridge (13°E to 47°E). J. Petrol. 46, 2427–2464.
Kay, R.W., 1978. Aleutian magnesian andesites: melts from subducted Pacific crust. J. Volcanol. Geotherm. Res. 4, 117–132.
Kay, R.W., 1980. Volcanic arc magma genesis: implications for element recycling in the crust–upper mantle system. J. Geol. 88, 497–522.
Kay, S.M., Kay, R.W., 1985. Aleutian tholeiitic and calc-alkaline magma series, I: the mafic phenocrysts. Contrib. Mineral. Petrol. 90, 276–290.
Kelemen, P.B., 1995. Genesis of high Mg# andesites and the continental crust. Contrib. Mineral. Petrol. 120, 1–19.
Kelley, K.A., Plank, T., Ludden, J.N., Staudigel, H., 2003. Composition of altered oceanic crust at ODP Sites 801 and 1149. Geochem. Geophys. Geosyst. 4, 21.
Kempton, P.D., Pearce, J.A., Barry, T.L., Fitton, J.G., Langmuir, C., Christi, D.M., 2002. Sr–Nd–Pb–Hf isotope results from ODP leg 187: evidence for mantle dynamics of the Australian–Antarctic discordance and origin of the Indian MORB source. Geochemistry Geophysics Geosystems 3, 1–35.
Kepezhinskas, P., McDermott, F., Defant, M.J., Hochstaedter, A., Drummond, M.S., Hawkesworth, C.J., Koloskov, A., Maury, R.C., Bellon, H., 1997. Trace element and Sr–Nd–Pb isotopic constraints on a three-component model of Kamchatka arc petrogenesis. Geochim. Cosmochim. Acta 61, 577–600.
Kersting, A.B., Arculus, R.J., 1994. Klyuchevskoy Volcano, Kamchatka, Russia: the role of high-flux, recharged, tapped and fractionated magma chamber(s) in the genesis of high-Al_2O_3 from high-MgO basalt. J. Petrol. 35, 1–42.
Kersting, A.B., Arculus, R.J., 1995. Pb isotope composition of Klyuchevskoy volcano, Kamchatka and North Pacific sediments: implications for magma genesis and crustal recycling in the Kamchatkan arc. Earth Planet. Sci. Lett. 136, 133–148.
Kessel, R., Schmidt, M.W., Ulmer, P., Pettke, T., 2005. Trace element signature of subduction-zone fluids, melts and supercritical liquids at 120–180 km depth. Nature 437, 724–727.
Kimura, J.I., Yoshida, T., 2006. Contributions of slab fluid, mantle wedge and crust to the origin of Quaternary lavas in the NE Japan arc. J. Petrol. 47, 2185–2232.
Kimura, J.I., Kent, A.J.R., Rowe, M.C., Katakuse, M., Nakano, F., Hacker, B.R., van Keken, P.E., Kawabata, H., Stern, R.J., 2010. Origin of cross chain geochemical variation in Quaternary lavas from the northern Izu arc: using a quantitative mass balance approach to identify mantle sources and mantle wedge processes. Geochem. Geophys. Geosyst. 11.
Klein, E.M., Langmuir, C.H., Zindler, A., Staudigel, H., Hamelin, B., 1988. Isotope evidence of a mantle convection boundary at the Australian–Antarctic discordance. Nature 333, 623–629.
Labanieh, S., Chauvel, C., Germa, A., Quidelleur, X., 2012. Martinique: a clear case for sediment melting and slab dehydration as a function of distance to the trench. J. Petrol. 53, 2441–2464.
Lange, R.A., Carmichael, I.S.E., 1996. The Aurora volcanic field, California–Nevada: oxygen fugacity constraints on the development of andesitic magma. Contrib. Mineral. Petrol. 125, 167–185.
Lees, J.M., VanDecar, J., Gordeev, E., Ozerov, A., Brandon, M., Park, J., Levin, V., 2007. Three dimensional images of the Kamchatka–Pacific plate cusp. Volcanism and Subduction: The Kamchatka Region. Geophysical Monograph Series 172, pp. 65–75.
Macdougall, J.K., Lugmair, G.W., 1986. Sr and Nd isotopes in basalts from the East Pacific Rise: significance for mantle heterogeneity. Earth Planet. Sci. Lett. 77, 273–284.
Mahoney, J.J., Sinton, J.M., Kurz, M.D., Macdougall, J.D., Spencer, K.J., Lugmair, G.W., 1994. Isotope and trace element characteristics of a super-fast spreading ridge: East Pacific rise, 13°–23°S. Earth Planet. Sci. Lett. 121, 173–193.
Mahoney, J.J., Graham, D.W., Christie, D.M., Johnson, K.T.M., Hall, L.S., Vonderhaar, D.L., 2002. Between a hotspot and a cold spot: isotopic variation in the southeast Indian Ridge asthenosphere, 86°E–118°E. J. Petrol. 43, 1155–1176.
Meyzen, C.M., Blichert-Toft, J., Ludden, J.N., Humler, E., Mével, C., Albarède, F., 2007. Isotopic portrayal of the Earth's upper mantle flow field. Nature 447, 1069–1074.
Miyashiro, A., 1974. Volcanic rock series in island arcs and active continental margins. Am. J. Sci. 274, 321–355.
Moore, G.W., Bogdanov, N.A., Drummond, K.J., Golovchenko, X., Larson, R.L., Pitman III, W. C., Rinehart, W.A., Siebert, L., Simkin, T., Tilman, S.M., Uyeda, S., 1992. Plate-tectonic map of the Circum-Pacific Region, Arctic Sheet. Circum-Pacific Map Series. United States Geological Survey, p. 20.
Morris, P.A., 1995. Slab melting as an explanation of Quaternary volcanism and aseismicity in southwest Japan. Geology 23 (5), 395–398.
Münker, C., Weyer, S., Scherer, E., Mezger, K., 2001. Separation of high field strength elements (Nb, Ta, Zr, Hf) and Lu from rock samples for MC-ICPMS measurements. Geochem. Geophys. Geosyst. 2 (no. 12).
Nakamura, E., Campbell, I.H., Sun, S.S., 1985. The influence of subduction processes on the geochemistry of Japanese alkaline basalts. Nature 316, 55–58.
Newsom, H.E., White, W.M., Jochum, K.P., Hofmann, A.W., 1986. Siderophile and chalcophile element abundances in oceanic basalts, Pb-isotope evolution and growth of the Earths core. Earth Planet. Sci. Lett. 80, 299–313.
Niu, Y.L., Collerson, K., Batiza, R., Wendt, J., Regelous, M., 1999. Origin of enriched-type mid-ocean ridge basalt at ridges far from mantle plumes: the East Pacific Rise at 11°20′N. J. Geophys. Res. 104, 7067–7087.
Niu, Y.L., Regelous, M., Wendt, I.J., Batiza, R., O'Hara, M.J., 2002. Geochemistry of near-EPR seamounts: importance of source vs. process and the origin of enriched mantle component. Earth Planet. Sci. Lett. 199, 327–345.
Nowell, G.M., Kempton, P.D., Noble, S.R., Fitton, J.G., Saunders, A.D., Mahoney, J.J., Taylor, R. N., 1998. High precision Hf isotope measurements of MORB and OIB by thermal ionisation mass spectrometry: insights into the depleted mantle. Chem. Geol. 149, 211–233.
Ozerov, A.Y., 2000. The evolution of high-alumina basalts of the Klyuchevskoy, volcano, Kamchatka, Russia, based on microprobe analyses of mineral inclusions. J. Volcanol. Geotherm. Res. 95, 65–79.
Ozerov, A.Y., Ariskin, A.A., Kyle, P., Bogoyavlenskaya, G.E., Karpenko, S.F., 1997. Petrological–Geochemical model for genetic relationships between basaltic and andesitic magmatism of Klyuchenskoi and Bezymyannyi volcanoes, Kamchatka. Petrology 5, 550–569.
Pearce, J.A., Kempton, P.D., Nowell, G.M., Noble, S.R., 1999. Hf–Nd element and isotope perspective on the nature and provenance of mantle and subduction components in western Pacific arc-basin systems. J. Petrol. 40, 1579–1611.
Petford, N., Gallagher, K., 2001. Partial melting of mafic (amphibolitic) lower crust by periodic influx of basaltic magma. Earth Planet. Sci. Lett. 193, 483–499.
Petford, N., Atherton, M., 1996. Na-rich partial melts from newly underplated basaltic crust: the Cordillera Blanca batholith, Peru. Journal of Petrology 37, 1491–1521.
Pineau, F., Semet, M.P., Grassineau, N., Okrugin, V.M., Javoy, M., 1999. The genesis of the stable isotope (O, H) record in arc magmas: the Kamchatka's case. Chem. Geol. 135, 93–124.
Plank, T., 2014. The chemical composition of subducting sediments, Treatise on GeochemistrySecond Edition. ,pp. 607–629 http://dx.doi.org/10.1016/8978-0-08-095975-7-00319-3.
Plank, T., Langmuir, C.H., 1998. The chemical composition of subducting sediment and its consequences for the crust and mantle. Chem. Geol. 145, 325–394.
Ponomareva, V.V., Pevzner, M., Melekestsev, I.V., 1998. Large debris avalanches and associated eruptions in the Holocene eruptive history of Shiveluch Volcano, Kamchatka, Russia. Bull. Volcanol. 59, 490–505.
Ponomareva, V.V., Churikova, T., Melekestsev, I.V., Braitseva, O.A., Pevzner, M., Sulerzhitsky, L.D., 2007. Late Pleistocene–Holocene volcanism on the Kamchatka Peninsula, northwest Pacific region. In: Eichelberger, J., Gordeev, E., Izbekov, P., Kasahara, M., Lees, J. (Eds.), Geophysical Monograph 172, Volcanism and Subduction: The Kamchatka Region. American Geophysical Union, Washington, DC, pp. 165–198.
Portnyagin, M., Hoernle, K., Avdeiko, G., Hauff, F., Werner, R., Bindeman, I.N., Uspensky, V., Garbe-Schönber, D., 2005. Transition from arc to oceanic magmatism at the Kamchatka–Aleutian junction. Geology 33, 25–28.

Portnyagin, M., Hoernle, K., Plechov, P., Mironov, N., Khubunaya, S., 2007a. Constraints on mantle melting and composition of slab components in volcanic arcs from volatiles (H_2O, S, Cl, F) and trace elements in melt inclusions from the Kamchatka Arc. Earth Planet. Sci. Lett. 255 (1–2), 53–69.

Portnyagin, M., Bindeman, I., Hoernle, K., Hauff, F., 2007b. Geochemistry of primitive lavas of the Central Kamchatka Depression: magma generation at the edge of the Pacific Plate. In: Eichelberger, J., Gordeev, E., Izbekov, P., Kasahara, M., Lees, J. (Eds.), Geophysical Monograph 172, Volcanism and Subduction: The Kamchatka Region. American Geophysical Union, Washington, DC, pp. 199–239.

Pyle, D.G., Christie, D.M., Mahoney, J.J., 1992. Resolving an isotopic boundary within the Australian–Antarctic Discordance. Earth Planet. Sci. Lett. 112, 161–178.

Ranero, C.R., Sallarés, V., 2004. Geophysical evidence for hydration of the crust and mantle of the Nazca plate during bending at the north Chile trench. Geology 32 (7), 549–552.

Ranero, C.R., Morgan, J.P., McIntosh, K., Reichert, C., 2003. Bending-related faulting and mantle serpentinization at the Middle America trench. Nature 425, 367–373.

Rapp, R.P., Watson, E.B., 1995. Dehydration melting of metabasalt at 8–32 kbar: implications for continental growth and crust–mantle recycling. J. Petrol. 36, 891–931.

Rapp, R.P., Watson, E.B., Miller, C.F., 1991. Partial melting of amphibolite/eclogite and the origin of Archean trondhjemites and tonalites. Precambrian Res. 51, 1–25.

Regelous, M., Niu, Y., Wendt, J.I., Batiza, R., Greig, A., Collerson, K.D., 1999. Variations in the geochemistry of magmatism on the East Pacific Rise at 10°30′N since 800 ka. Earth Planet. Sci. Lett. 168.

Romick, J.D., Kay, S.M., Kay, R.W., 1992. The influence of amphibole fractionation on the evolution of calc-alkaline andesite and dacite tephra from the central Aleutians, Alaska. Contrib. Mineral. Petrol. 112 (1), 101–118.

Rooney, T.O., Franceschi, P., Hall, C.M., 2010. Water-saturated magmas in the Panama Canal region: a precursor to adakite-like magma generation. Contrib. Mineral. Petrol. 161, 373–388.

Rudnick, R.L., Fountain, D.M., 1995. Nature and composition of the continental crust: a lower crustal perspective. Rev. Geophys. 33, 267–309.

Rushmer, T., 1991. Partial melting of two amphibolites: contrasting experimental results under fluid-absent conditions. Contrib. Mineral. Petrol. 107, 41–59.

Ryan, J.G., Morris, J., Tera, F., Leeman, W.P., A., T., 1995. Cross-arc geochemical variations in the Kurile Arc as a function of slab depth. Science 270, 625–627.

Saha, A., Basu, A., Jacobsen, S., Poreda, R., Yin, Q., Yogodzinski, G.M., 2005. Slab devolatilization and Os and Pb mobility in the mantle wedge of the Kamchatka arc. Earth Planet. Sci. Lett. 236, 182–194.

Sakuyama, M., Nesbitt, R.W., 1986. Geochemistry of the Quaternary volcanic rocks of the northeast Japan arc. J. Volcanol. Geotherm. Res. 29, 413–450.

Salters, V.J.M., Hart, S.R., 1991. The mantle sources of ocean ridges, islands and arcs; the Hf-isotope connection. Earth and Planetary Science Letters 104 (2–4), 364–380.

Salters, V.J.M., 1996. The generation of mid-ocean ridge basalts from the Hf and Hd isotope perspective. Earth Planet. Sci. Lett. 141, 109–123.

Salters, V.J.M., Stracke, A., 2003. Composition of the depleted mantle. Geochem. Geophys. Geosyst. 5. http://dx.doi.org/10.1029/2003GC000597.

Salters, V.J.M., White, W.M., 1998. Hf isotope constrains on mantle evolution. Chem. Geol. 145, 447–460.

Savov, I.P., Ryan, J.G., D'Antonio,, M., Kelley, K., Mattie, P., 2005. Geochemistry of serpentinized peridotites from the Mariana Forearc-Conical Seamount, ODP Leg 125: implications for the elemental recycling at subduction zones. Geochem. Geophys. Geosyst. 6 (4), Q04J15. http://dx.doi.org/10.1029/2004GC000777.

Savov, I.P., Ryan, J.G., D'Antonio,, M., Fryer, P., 2005. Shallow slab fluid release across and along the Mariana arc-basin system: Insights from geochemistry of serpentinized peridotites from the Mariana Forearc. J. Geophys. Res. http://dx.doi.org/10.1029/2006JB004749.

Schmidt, M.W., Vielzeuf, D., Auzanneau, E., 2004. Melting and dissolution of subducting crust at high pressures: the key role of white mica. Earth Planet. Sci. Lett. 228, 65–84.

Selyangin, O.B., 1993. Mutnovsky Volcano, Kamchatka: new evidence on structure, evolution, and future activity. Volcanol. Seismol. 15, 17–38.

Selyangin, O.B., 2009. Wonderful World of Mutnovsky and Gorely Volcanoes: Volcanologic and Traveller's Guide. Novaja kniga, Petropavlovsk-Kamchatsky (108 pp.).

Shibata, T., Nakamura, E., 1997. Across-arc variations of isotope and trace element compositions from Quaternary basaltic volcanic rocks in northeastern Japan: implications for interaction between subducted oceanic lab and mantle wedge. J. Geophys. Res. 102, 8051–8064.

Shimoda, G., Tatsumi, Y., Nohda, S., Ishizaka, K., Jahn, B.M., 1998. Setouchi high-Mg andesites revisited: geochemical evidence for melting of subducting sediments. Earth Planet. Sci. Lett. 160, 479–492.

Sims, K.W.W., Goldstein, S.J., Blichert-Toft, J., Perfit, M.R., Kelemen, P., Fornari, D.J., Michael, P.M., Murrell, M.T., Hart, S.R., DePaulo, D.J., Layne, G., Ball, L., Jull, M., Bender, J., 2002a. Chemical and isotopic constraints on the generation and transport of magma beneath the East Pacific Rise. Geochim. Cosmochim. Acta 66, 3481–3504.

Sims, K.W., Goldstein, S.J., Blichert-Toft, J., Perfit, M.R., Kelemen, P.B., Fornari, D.J., Michael, P., Murrell, M.T., Hart, S.R., DePaolo, D.J., Layne, G.D., Ball, L., Jull, M., Bender, J., 2002b. Chemical and isotopic constraints on the generation and transport of magma beneath the East Pacific Rise. Geochim. Cosmochim. Acta 66, 3481–3504.

Skora, S., Blundy, J., 2010. High-pressure hydrous phase relations of radiolarian clay and implications for the involvement of subducted sediment in arc magmatism. J. Petrol. 51, 2211–2243.

Spandler, C., Mavrogenes, J., Hermann, J., 2007. Experimental constraints on element mobility from subducted sediments using high-P synthetic fluid/melt inclusions. Chem. Geol. 239, 228–249.

Stern, R.J., Jackson, M.C., Freyer, P., Ito, E., 1993. O, Sr Nd and Pb isotoic composition of the Kasuga cross-chain in the Mariana arc: a new perspective on the K–h relationship. Earth Planet. Sci. Lett. 119, 459–475.

Stormer Jr., J.C., Nicholls, J., 1978. XLFRAC: a program for the interactive testing of magma differentiation models. Comput. Geosci. 4 (2), 143–159.

Sun, S.S., McDonough, W.F., 1989. Chemical and isotopic systematic of oceanic basalts: implications for mantle compositions and processes. In: Saunders, A.D., Norry, M.J. (Eds.), Magmatism in the Ocean Basins. Geological Society of London Special Publications 42, pp. 313–345.

Tatsumi, Y., Hamilton, D.L., Nesbitt, R.W., 1986. Chemical characteristics of fluid phase released from a subducted lithosphere and origin of arc magmas: evidence from high-pressure experiments and natural rocks. J. Volcanol. Geotherm. Res. 29, 293–309.

Tepper, J.H., Nelson, B.K., Bergantz, G.W., Irving, A.J., 1993. Petrology of the Chilliwack Batholith, North Cascades, Washington: generation of calc-alkaline granitoids by melting of mafic lower crust with variable water fugacity. Contrib. Mineral. Petrol. 113, 333–351.

Todd, E., Gill, J., Wysoczanski, R., Handler, M., Wright, I., Gamble, J., 2010. Sources of constructional cross-chain volcanism in the southern Havre Trough: new insights from HFSE and REE concentration and isotope systematics. Geophysics, Geochemistry, Geosystems 11. http://dx.doi.org/10.1029/2009GC002888.

Tollstrup, D., Gill, J.B., Prinkey, D., Williams, R., Tamura, Y., Ishizuka, O., 2010. Across-arc geochemical trends in the Izu–Bonin arc: contributions from the subducting slab, revisited. Geochem. Geophys. Geosyst. 11. http://dx.doi.org/10.1029/2009GC002847.

Turner, S., Hawkewsworth, C., van Calsteren, P., Heath, E., Macdonald, R., Black, S., 1996. U-series isotopes and destructive plate margin magma genesis in the Lesser Antilles. Earth Planet. Sci. Lett. 142, 191–207.

Turner, S., McDermott, F., Hawkesworth, C., Kepezhinskas, P., 1998. A U-series study of lavas from Kamchatka and the Aleutians: constraints on source composition and melting processes. Contrib. Mineral. Petrol. 133, 217–234.

Turner, S., Bourdon, B., Gill, J.B., 2003. Insights into magma genesis at convergent margins from U-series isotopes. Rev. Mineral. Geochem. 52, 255–315.

Turner, S., Sims, K.W.W., Reagan, M., Cook, C., 2007. A 210Pb-226Ra-230Th 238U study of Klyuchevskoy and Bezymianny volcanoes, Kamchatka. Geochim. Cosmochim. Acta 71, 4771–4785.

Turner, S., Caulfield, J., Rushmer, T., Turner, M., Cronin, S., Smith, I., Handley, H., 2012. Magma evolution in the primitive, intra-oceanic Tonga Arc: rapid petrogenesis of dacites at Fonualei Volcano. J. Petrol. 53, 1231–1253.

Viccaro, M., Giuffrida, M., Nicotra, E., Ozerov, A.Y., 2012. Magma storage, ascent and recharge history prior to the 1991 eruption at Avachinsky Volcano, Kamchatka, Russia: inferences on the plumbing system geometry. Lithos 140–141, 11–24.

Vlastélic, I., Aslanian, D., Dosso, L., Bougault, H., Olivet, J.L., Geli, L., 1999. Large-scale chemical and thermal division of the Pacific mantle. Nature 399, 345–350.

Volynets, O.N., 1994. Geochemical types, petrology, and genesis of Late Cenozoic volcanic rocks from the Kurile–Kamchatka island-arc system. Int. Geol. Rev. 36, 373–405.

Volynets, O.N., Ponomareva, V.V., Babansky, A.D., 1997. Magnesian basalts of Shiveluch andesite volcano, Kamchatka. Petrology 5, 83–96.

Volynets, O.N., Melekestsev, I.V., Ponomareva, V.V., Yogodzinski, G.M., 1999. Kharchinsky and Zarechny volcanoes, unique centers of Late Pleistocene magnesian basalts in Kamchatka: composition of erupted rocks. Volcanol. Seismol. 21, 45–66.

Volynets, O.N., Babansky, A., Goltsman, Y.V., 2000. Variations in isotopic and trace element composition of lava from volcanoes of the Northern Group, Kamchatka, in relation to specific features of subduction. Geochem. Int. 38, 974–989.

Volynets, A.O., Churikova, T.G., Wörner, G., Gordeychik, B.N., Layer, P., 2010. Mafic Late Miocene–Quaternary volcanic rocks in the Kamchatka back arc region: implication for subduction geometry and lab history at the Pacific–Aleutian junction. Contrib. Mineral. Petrol. 159, 659–687.

Wanless, V.D., Perfit, M.R., Ridley, W.I., Klein, E., 2010. Dacite petrogenesis on mid-oceanic ridges: evidence for oceanic crustal melting and assimilation. J. Petrol. 51, 2377–2410.

Waters, C.L., Sims, K.W.W., Perfit, M.R., Blichert-Toft, J., Blusztajn, J., 2011. Perspective on the genesis of E-MORB from chemical and isotopic heterogeneity at 9°–10°N East Pacific Rise. J. Petrol. 52, 565–602.

Weis, D., Kieffer, B., Maerschalk, C., Barling, J., De Jong, J., Williams, G., Hanano, D., Pretorius, W., Mattielli, N., Scoates, J.S., Goolaerts, A., Friedman, R., Mahoney, J.B., 2006. High-precision isotopic characterization of USGS reference materials by TIMS and MC-ICP-MS. Geochem. Geophys. Geosyst. 7, Q08006. http://dx.doi.org/10.1029/2006GC001283.

Wendt, J.I., Regelous, M., Niu, Y., Hekinian, R., Collerson, K.D., 1999. Geochemistry of lavas from the Garrett Transform Fault: insights into mantle heterogeneity beneath the eastern Pacific. Earth Planet. Sci. Lett. 173, 271–284.

White, W.M., Albarede, F., Telouk, P., 2000. High-precision analysis of Pb isotopic ratios using multi-collector ICP-MS. Chem. Geol. 167, 257–270.

Widom, E., Kepezhinkas, P.K., Defant, M., 2003. The nature of metasomatism in the sub-arc mantle wedge: evidence from Re–Os isotopes in Kamchatka peridotite xenoliths. Chem. Geol. 196, 283–306.

Workman, R.K., Hart, S.R., 2005. Major and trace element composition of the depleted MORB mantle (DMM). Earth Planet. Sci. Lett. 231 (1), 53–72.

Yogodzinski, G.M., Volynets, O.N., Koloskov, A.V., Seliverstov, N.I., Matvenkov, V.V., 1994. Magnesian andesites and the subduction component in a strongly calc-alkaline series at Piip Volcano, far western Aleutians. J. Petrol. 35, 163–204.

Yogodzinski, G.M., Kay, R.W., Volynets, O.N., Koloskov, A.V., Kay, S.M., 1995. Magnesian andesite in the western Aleutian Komandorsky region: implications for slab melting and processes in the mantle wedge. Geol. Soc. Am. Bull. 107, 505–519.

Yogodzinski, G.M., Lees, J.M., Churikova, T.G., Dorendorf, F., Wörner, G., Volynets, O.N., 2001. Geochemical evidence for the melting of subducting oceanic lithosphere at plate edges. Nature 409, 500–504.

Yogodzinski, G.M., Brown, S.T., Kelemen, P.B., Vervoort, J.D., Portnyagin, M., Sims, K.W.W., Hoernle, K., Jicha, B., Werner, R., 2014. The role of subducted basalt in the source of island arc magmas: evidence from seafloor lavas of the western Aleutians. Journal of Petrology in press.

Yu, Y., Xu, W., Wang, C., 2014. Experimental studies of melt–peridotite reactions at 1–2 GPa and 1250–1400C and their implications for transforming the nature of lithospheric mantle and for high-Mg signatures in adakitic rocks. Sci. China Earth Sci. 57, 415–427.